Towards a Fluid-Structure Interaction solver for problems with large deformations within the open-source SU2 suite

Ruben Sanchez,* Rafael Palacios,†
Imperial College, London, SW7 2AZ, United Kingdom

Thomas D. Economon,‡ Heather L. Kline,§ Juan J. Alonso,¶
Stanford University, Stanford, CA, 94305, USA

and Francisco Palacios‖
The Boeing Company, Long Beach, CA, 90808, USA

This paper describes a new framework for Fluid-Structure Interaction (FSI) modelling within the open-source code SU2. SU2 has been developed to solve complex, multi-physics problems described by Partial Differential Equations (PDEs), with an emphasis on problems involving aerodynamic shape optimization. Due to its modularity, the code provides an appropriate infrastructure for the solution of physical problems in several disciplines. This work provides SU2 with new tools that expand its capabilities in the fields of structural analysis and FSI. The focus will be on geometrically-nonlinear deformable solids in low-speed external flows.

A Finite Element (FE) structural solver, able to deal with geometrical and material non-linearities in a static and a dynamic setting, has been built within the framework of SU2 alongside the existing solvers. Following the original object-oriented architecture in C++, a new structure compliant with the CFD solver has been developed. These new features will serve as a basis for future developments of FE-based strategies for the solution of PDEs. The structural solver has been coupled with the original fluid solver in SU2 using a partitioned approach. The structure of the code was fully recast to allow analysis across multiple zones and physical problems, currently limited to problems involving fluid and structural analysis. Both loosely- and strongly-coupled strategies are available for the solution of the coupled FSI problem.

Finally, the validity of the implementations is assessed by studying the behavior of a rigid square with a flexible cantilever at low Reynolds number. The results obtained demonstrate the capabilities of these new developments and further address the physics behind this benchmark problem.

*Graduate Student, Department of Aeronautics, 363A Roderic Hill Building; r.sanchez-fernandez14@imperial.ac.uk. AIAA Student Member.
†Reader, Department of Aeronautics. AIAA Senior Member.
‡Postdoctoral Scholar, Department of Aeronautics & Astronautics. AIAA Senior Member.
§PhD. Candidate, Department of Aeronautics & Astronautics. AIAA Student Member.
¶Professor, Department of Aeronautics & Astronautics. AIAA Associate Fellow.
‖Engineer, Advanced Concepts Group. AIAA Senior Member.

Nomenclature

ρ	Density
Ω	Domain
Γ	Boundary
$\mathbf{n}$	Vector normal to a surface

Fluid variables

$\mathbf{v}$	Velocity
E	Total energy per unit mass
p	Pressure
μ_f	Fluid viscosity
C_p	Specific heat
$\bar{\bar{\boldsymbol{\tau}}}$	Viscous stress tensor
$\mathbf{U}$	Vector of conservative variables
$\mathbf{F^c}$	Vector of convective fluxes
$\mathbf{F^v}$	Vector of viscous fluxes
$\boldsymbol{\lambda}_f$	Fluid tractions over the FSI interface

Mesh variables

$\mathbf{u}_\Omega$	Nodal displacements on the fluid mesh
$\dot{\mathbf{u}}_\Omega$	Nodal velocities on the fluid mesh
$\mathbf{K}^m$	Stiffness matrix of the mesh deformation problem

Structural variables

E	Young's modulus
ν	Poisson ratio
λ, μ	Lame constants
$\mathbf{M}$	Mass matrix
$\mathbf{K}$	Stiffness matrix
$\mathbf{K}_c$	Constitutive term of the stiffness matrix
$\mathbf{K}_s$	Stress term of the stiffness matrix
$\mathbf{F}_e$	Vector of external forces
$\mathbf{T}$	Vector of internal equivalent nodal forces
$\mathbf{N}$	Element shape functions
$\mathbf{B}$	Matrix of shape function gradients
$\mathbf{u}$	Nodal displacements
$\dot{\mathbf{u}}$	Nodal velocities
$\ddot{\mathbf{u}}$	Nodal accelerations
$\mathbf{F}$	Deformation gradient
$\mathbf{S}$	Second Piola-Kirchhoff stress tensor
$\mathbf{D}$	Constitutive matrix
$\boldsymbol{\sigma}$	Cauchy stress tensor
$\mathbf{b}$	Left Cauchy-Green deformation tensor
J	Jacobian of the deformation gradient
β, γ	Newmark method parameters
α_m, α_f	Generalized-α method parameters
Ψ	Free energy function
$\boldsymbol{\lambda}_s$	Tractions applied on the structural side of the FSI interface

Coupled problem

$\mathscr{F}(\cdot)$	Dirichlet-to-Neumann fluid operator
$\mathscr{S}(\cdot)$	Dirichlet-to-Neumann structural operator
ω	Aitken's dynamic relaxation parameter
$\mathscr{R}_\mathbf{u}$	Residual on the FSI interface
ϵ	Tolerance criterion

Interpolation problem

$\mathbf{H}$	Transformation matrix
$\Phi(\mathbf{x})$	Radial basis function
$\mathbf{x}$	Spatial coordinates
r	Radius

Subscript

f	Fluid
s	Structure
a, b	Nodes of the FE discretization
e	Essential boundary condition
n	Natural boundary condition
i	FSI interface

Superscript

n	Current iteration
$n-1$	Previous iteration
$t+\Delta t$	Current time step
t	Previous time step

I. Introduction

Computational Fluid-Structure Interaction with complex flow and/or structural behavior is an area of active research in diverse subjects such as computational aeroelasticity,[1–5] biomechanics,[6,7] and turbomachinery.[8,9] Each particular problem has its own requirements in terms of the physics involved, and as a result several methods have arisen specifically oriented to solve them.[10–19] Given the complex physics involved in the solution of computational FSI, where strong non-linearities may occur both in each domain separately and in the interaction itself, the performance of the solvers employed in highly parallel environments becomes a key issue, specially when addressing large problems. Therefore, both accuracy and efficiency in the solvers become unavoidable requirements for the computational study of this problem.

It has been found worthy to explore the development and employment of new tools that can give adequate response to these requirements from a general point of view. In this sense, the open-source SU2 software suite[20,21] sets a very appropriate starting point for the development of a new, integrated Fluid-Structure

Interaction solver. SU2 consists of a set of tools that have been developed from the ground up to solve complex multiphysics Partial Differential Equation-based (PDE) problems, using unstructured meshes while including shape design and optimization procedures. The code is highly encapsulated and composed of a set of C++ routines organized in a modular way, thus allowing for the integration of new implementations in a structured and efficient way.

Although originally developed as a Computational Fluid Dynamics (CFD) tool for treating aerodynamic shape optimization problems in compressible flows, the code is now being used for analysis and design purposes in several disciplines such as chemical, mechanical, industrial and naval engineering.[22] Economon *et al.*[22] have recently summarized the approach of the SU2 team to code optimization, in order to improve the performance and scalability of the suite by executing the CFD solver on highly parallel architectures, identifying some of the typical bottlenecks and proposing algorithms suitable for large-scale simulations. This ability to handle large-scale problems, together with the modularity and open-source nature of the code, make SU2 a unique platform for the implementation of an efficient and robust computational FSI solver. This paper presents the current status of that project.

This paper is organized as follows. Section II summarizes the governing equations and the interface coupling condition, and assesses the solution methods that have been considered for the implementation. Section III describes the structure of the code. The results obtained in the study of a cantilever beam undergoing large deformations under the action of a vortical flow are presented in section IV, demonstrating the potential of the solver to become a general tool in FSI. Finally, section V summarizes the contributions and main findings of this work.

II. Background

From a physical point of view, the Fluid-Structure Interaction problem may be described as the analysis of two different fields (fluid and structure) governed by their own constitutive equations, and interacting with each other over a common interface. The fluid conservative variables are $(\rho_f, \rho\mathbf{v}, \rho E)$, being ρ_f the density, $\mathbf{v}$ the velocity and E the energy, while in the solid domain, the variables are the displacements $\mathbf{u}$ and velocities $\dot{\mathbf{u}}$ with respect to an inertial observer. In order for the problem to be fully coupled (Fig. 1), the fluid pressures p_Γ and viscous stresses $\bar{\bar{\boldsymbol{\tau}}}_\Gamma$ from the fluid field are applied onto the structure at the common interface, resulting in structural displacements and velocities on the common boundary $(\mathbf{u}_\Gamma, \dot{\mathbf{u}}_\Gamma)$ that modify the external shape of the structure, thus affecting the fluid field.

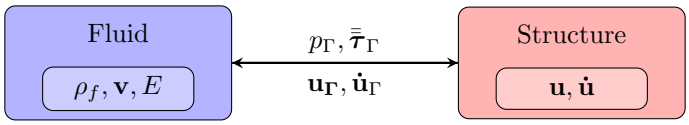

Figure 1. Fluid-Structure Interaction problem

In numerical solutions for unsteady flows with dynamic meshes, it is necessary to introduce a third field in the problem, the computational grid of the fluid, where the variables are the displacements $\mathbf{u}_\Omega$ and velocities $\dot{\mathbf{u}}_\Omega$ of its nodes. Moreover, it is needed to define the strategy to be adopted in order to couple the computational fluid and structural solvers.

There are two main coupling architectures.[23] On the one hand, it is possible to adopt a *monolithic approach*, thus solving simultaneously the fluid and structural equations while imposing the interface conditions. This approach is robust and accurate, and has been proven to be more efficient in some applications in biomechanics.[15,24] Nevertheless, it requires the development of highly specialized code, a challenging task that in most cases leads to solvers that, according to Piperno *et al.*,[25] are not optimal.

A *partitioned approach*, on the other hand, permits the employment of an adequate solver for each subproblem,[26] and is simpler and easier to implement. This will be the procedure adopted in this work, as we are interested in maintaining the modularity of SU2 while developing a very specific structural solver able to deal with problems involving very large deformations and complex material behavior. Therefore, it has been necessary to assess the different approaches for temporal integration and spatial interpolation of the fields on the interface in order to guarantee the stability and accuracy of the scheme. The adoption of a partitioned approach introduces a new field into the problem, which is the interface, upon which the coupling conditions will be applied (Fig. 2).

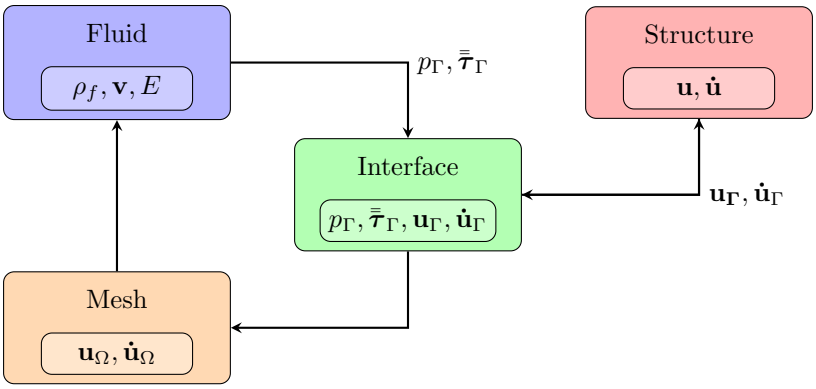

Figure 2. Partitioned Fluid-Structure Interaction problem

II.A. Fluid domain

The behavior of a viscous, compressible, Newtonian flow is governed by the Navier-Stokes equations, assuming an Eulerian description of the motion. In FSI problems, there are moving boundaries in the domain which make it necessary to account for the displacements on the mesh. Therefore, the Navier-Stokes equations have been reformulated in an Arbitrary Lagrangian-Eulerian (ALE) framework.[20,21,27,28] Defining a conservative variable $\mathbf{U} = (\rho_f, \rho\mathbf{v}, \rho E)$, it is possible to write the PDE system as[20]

$$\frac{\partial \mathbf{U}}{\partial t} + \nabla \cdot \mathbf{F^c}_{ALE}(\mathbf{U}) = \nabla \cdot \mathbf{F^v}(\mathbf{U}) \qquad \text{in } \Omega_f \times [0,t] \tag{1}$$

where $\mathbf{F^c_{ALE}}(\mathbf{U})$ is the vector of convective fluxes and $\mathbf{F^v}(\mathbf{U})$ corresponds to the viscous fluxes, defined by

$$\mathbf{F^c_{ALE}}(\mathbf{U}) = \begin{pmatrix} \rho_f(\mathbf{v} - \dot{\mathbf{u}}_\mathbf{\Omega}) \\ \rho_f \mathbf{v} \otimes (\mathbf{v} - \dot{\mathbf{u}}_\mathbf{\Omega}) + \bar{\bar{I}}p \\ \rho_f(\mathbf{v} - \dot{\mathbf{u}}_\mathbf{\Omega})E + p\mathbf{v} \end{pmatrix}, \qquad \mathbf{F^v}(\mathbf{U}) = \begin{pmatrix} \mathbf{0} \\ \bar{\bar{\boldsymbol{\tau}}} \\ \bar{\bar{\boldsymbol{\tau}}} \cdot \mathbf{v} + \mu_f C_p \nabla T \end{pmatrix} \tag{2}$$

being ρ_f the fluid density, $\mathbf{v} = (v_1, v_2, v_3)$ the vector of flow velocities in a Cartesian coordinate system, E the total energy of the flow per unit mass, $\bar{\bar{\boldsymbol{\tau}}}$ the viscous stress tensor, μ_f the fluid viscosity, C_p the specific heat, T the temperature and $\dot{\mathbf{u}}_\mathbf{\Omega}$ the velocities of the nodes of the grid.

In order to define the solution of $\mathbf{U}$, it is necessary to prescribe the boundary conditions on both the external and internal boundaries. For the external boundaries, it is possible to define either free-stream boundary conditions (far-field or near-field) or characteristic-based inlet or outlet conditions. For the interface boundary Γ, we will have to apply wall boundary conditions. As the interface is moving, the velocity of the viscous flow on the surface has to be equal to the velocity of the surface. Moreover, we can also define equilibrium of the tractions on the interface on the fluid side. Thus, we have

$$\begin{cases} \mathbf{v}_f = \dot{\mathbf{u}}_{\Gamma_i} & \text{on } \Gamma_{f,i} \\ -p\mathbf{n}_f + \bar{\bar{\boldsymbol{\tau}}}_f \mathbf{n}_f = \boldsymbol{\lambda}_f & \text{on } \Gamma_{f,i} \end{cases} \tag{3}$$

where $\mathbf{v}_f$ is the velocity of the fluid on the interface, $\dot{\mathbf{u}}_{\Gamma_i}$ the velocity of the mesh nodes on the interface and $\mathbf{n}_f$ the dimensional, fluid normal outwards to the surface. A Dirichlet-to-Neumann non-linear operator for the fluid ($\mathscr{F}$) may be defined,[6,26] which associates the fluid tractions $\boldsymbol{\lambda}_f$ to the fluid displacements on the interface $\mathbf{u}_{\Gamma_f}$, as

$$\boldsymbol{\lambda}_f = \mathscr{F}(\mathbf{u}_{\Gamma_f}) \qquad \text{on } \Gamma_{f,i} \tag{4}$$

II.B. Structural domain

From the structural point of view, the continuum behavior is addressed by means of a Lagrangian description. The computational mesh follows the material particles,[28] thus allowing for tracking displacements, velocities and accelerations of the structure on the nodes. In the context of geometrically non-linear problems, the

governing equations are written as[29]

$$\rho_s \frac{\partial^2 \mathbf{u}}{\partial t^2} = \nabla(\mathbf{F} \cdot \mathbf{S}) + \rho_s \mathbf{f} \quad \text{in } \Omega_s \times [0, t] \tag{5}$$

where ρ_s is the structural density, $\mathbf{u}$ are the displacements of the solid, $\mathbf{F}$ the material deformation gradient, $\mathbf{S}$ the second Piola-Kirchhoff stress tensor and $\mathbf{f}$ the volume forces on the structural domain. In order to fully define the structural problem, it is also necessary to impose boundary conditions on the interface degrees of freedom, which may be classified[30] into essential (e) and natural (n) boundary conditions, where the former impose the solution $\mathbf{u}_{s,e}$ on a set of nodes of the interface and the latter apply tractions $\boldsymbol{\lambda}_{s,n}$ on the boundary. The boundary conditions for the problem can be written as

$$\begin{cases} \mathbf{u}_s = \mathbf{u}_{s,e} & \text{on } \Gamma_{s,e} \\ \bar{\bar{\boldsymbol{\sigma}}}_s \mathbf{n}_s = \boldsymbol{\lambda}_{s,n} & \text{on } \Gamma_{s,n} \end{cases} \tag{6}$$

where $\mathbf{n}_s$ is the dimensional, structural normal outwards to the surface. Analogous to the fluid domain, it is possible to define a Dirichlet-to-Neumann non-linear operator for the structural domain ($\mathscr{S}$), such that[6,26]

$$\boldsymbol{\lambda}_s = \mathscr{S}(\mathbf{u}_{\Gamma_s}) \qquad \text{on } \Gamma_{s,n} \tag{7}$$

As it will be further explained in the next section, it is interesting to define now the inverse operator $\mathscr{S}^{-1}$ as a Neumann-to-Dirichlet operator which, given the tractions $\boldsymbol{\lambda}_s$ maps the displacements $\mathbf{u}_s$ on Γ_i,

$$\mathbf{u}_{\Gamma_s} = \mathscr{S}^{-1}(\boldsymbol{\lambda}_s) \qquad \text{on } \Gamma_{s,n} \tag{8}$$

II.C. Coupling conditions

In order to close the equations defined in sections II.A and II.B, it is necessary to appropriately define the interface conditions.[1,6,26] Continuity is imposed over the common interface as

$$\mathbf{u}_f = \mathbf{u}_s = \mathbf{u}_\Gamma \tag{9}$$

On the other hand, the imposition of equilibrium conditions on $\Gamma \times [0, t]$ yields[26]

$$\boldsymbol{\lambda}_f + \boldsymbol{\lambda}_s = 0 \tag{10}$$

Having $\boldsymbol{\lambda}_f$ been defined on Eq. 4 and $\boldsymbol{\lambda}_s$ defined on Eq. 7. Combining equations 9 and 10, the problem can be rewritten as a Steklov-Poincaré equation[6,26]

$$\mathscr{F}(\mathbf{u}_\Gamma) + \mathscr{S}(\mathbf{u}_\Gamma) = 0 \tag{11}$$

This definition allows us to rewrite Eq. 11 as a fixed-point equation[26] using the definition in Eq. 8

$$\mathscr{S}^{-1}(-\mathscr{F}(\mathbf{u}_\Gamma)) = \mathbf{u}_\Gamma \tag{12}$$

For time-marching, the enforcement of the previous conditions will be addressed in the next section, as the requisites are different depending on the approach adopted.

II.D. Time coupling

Once adopted a partitioned approach, two possible strategies are available for the integration in time of the coupled problem. On the one hand, it is possible to adopt a loosely-coupled (staggered) procedure, which is an explicit approach consisting of sequentially solving the fluid and structure problems, advancing the solvers in time without enforcing the coupling conditions at the end of each time step. On the other hand, strongly-coupled strategies are also solved sequentially, but they require both solvers to meet the coupling conditions defined in section II.C in an implicit way, at the end of every single time step. Both of them will be briefly described in this section.

The loosely-coupled approach is the most elementary technique to solve the coupled problem, and due to its simple and modular implementation, it is widely used in Fluid-Structure Interaction problems, especially

in the field of computational aeroelasticity.[3,11,25,31] The simplest partitioned algorithm is the Conventional Serial Staggered[11] (CSS) procedure, which consists of one single solution of the Dirichlet-to-Neumann operator $\mathscr{F}(\mathbf{u})$ and the Neumann-to-Dirichlet inverse operator $\mathscr{S}^{-1}(\boldsymbol{\lambda})$ per time step. This is a collocation method, that is, each subfield has to be evaluated at the end of the same time window.[25,26]

while $t < T$ **do**
  Fluid solver: $\boldsymbol{\lambda}_{f,\Gamma}^{t+\Delta t}(p_\Gamma, \bar{\bar{\boldsymbol{\tau}}}_\Gamma) = \mathscr{F}(\mathbf{u}_\Gamma^t)$
  Structural solver: $\mathbf{u}_\Gamma^{t+\Delta t} = \mathscr{S}^{-1}(-\boldsymbol{\lambda}_{f,\Gamma}^{t+\Delta t})$
  $t \leftarrow t + \Delta t$;
end

Algorithm 1. Conventional Serial Staggered (CSS) method

As a result, kinematic continuity condition is not enforced, as the fluid is computed for $t + \Delta t$ with the position of the interface on time t. This results on a first order energy-accurate scheme,[25] regardless of the order of each subsolver. As a result of this lack of energy equilibrium, spurious energy is generated along the simulation, which may eventually result in large discrepancies in the prediction of pressures and viscous stresses on the interface.[32] It is possible to improve the accuracy of a staggered scheme by using a predictor for the structural displacements at the beginning of the simulation,[25] increasing the order of the scheme. The resulting algorithm is the so-called Generalized Serial Staggered (GSS).[25,26]

while $t < T$ **do**
  Predictor: $\tilde{\mathbf{u}}_\Gamma^{t+\Delta t} = \mathscr{P}_i(\mathbf{u}_\Gamma^t)$
  Fluid solver: $\boldsymbol{\lambda}_{f,\Gamma}^{t+\Delta t}(p_\Gamma, \bar{\bar{\boldsymbol{\tau}}}_\Gamma) = \mathscr{F}(\tilde{\mathbf{u}}_\Gamma^{t+\Delta t})$
  Structural solver: $\mathbf{u}_\Gamma^{t+\Delta t} = \mathscr{S}^{-1}(-\boldsymbol{\lambda}_{f,\Gamma}^{t+\Delta t})$
  $t \leftarrow t + \Delta t$;
end

Algorithm 2. Generalized Serial Staggered (GSS) method

Some instabilities and inaccuracies are inherent to loosely-coupled schemes and have been reported throughout the literature. In particular, the stability of these schemes is highly dependent on the density ratio ρ_s/ρ_f and the compressibility of the flow.[26,33,34] Incompressible flows combined with low density ratios generally require strongly coupled solvers due to the added-mass effect.[33,35] Moreover, thin-walled structures which undergo large deformations are also very sensitive to the quality of the solution scheme.[34] Some interesting attempts have been made to develop a higher order staggered scheme, as for example the Combined Interface Boundary Conditions (CIBC) method developed by Jaiman et. al,[32] or the works of Dettmer and Peric on a second-order staggered algorithm.[33]

In order to prevent the instabilities derived from the adoption of explicit schemes, it is common to adopt a strongly-coupled, implicit scheme.[12,26,34,36–39] These methods intend to eliminate the energy errors resulting of not enforcing the coupling conditions on the coupled time integration by imposing the conditions in section II.C at the end of each time step. One of the most extended strongly-coupled methods is the Block Gauss-Seidel (BGS) method, which implies the iterative solution of fluid and structural subsolvers within a time step until a tolerance criterion ϵ is met in the residual $\mathscr{R}_\mathbf{u} = \|\mathbf{u}_\Gamma^{n+1} - \mathbf{u}_\Gamma^n\| < \epsilon$.

Several authors have reported slow convergence or even divergence when the Fluid-Structure Interaction is strong, due for example to low density ratios, incompressible flows or large structural deformations.[34,38] Le Tallec and Mouro[12] proved that a fixed point algorithm without relaxation diverges for large deformable structures or small time steps. As a result, and in order to improve the convergence of the scheme, higher order displacement predictors have been used, combined with the employment of relaxation techniques.[26,34,37,39] The resultant procedure is described in algorithm 3.

In order to obtain the fastest convergence as possible, it is necessary to appropriately define the relaxation parameter ω^n. Küttler and Wall[37] carry out an interesting review on the possible values of ω^n. As the simplest option, a fixed relaxation parameter can prevent the computation from diverging, as long as it is small enough. Nevertheless, this choice generally results in a large number of iterations. Also, it is mentioned in the same reference that the optimal value for a fixed ω^n is problem-dependent. A simple and efficient option, as reported in several papers[34,37,39] is to use the dynamic Aitken's relaxation parameter.[40] If we define

$$\begin{aligned}\Delta\mathbf{u}_\Gamma^n &= \tilde{\mathbf{u}}_\Gamma^n - \mathbf{u}_\Gamma^{n-1} \\ \Delta\mathbf{u}_\Gamma^{n+1} &= \tilde{\mathbf{u}}_\Gamma^{n+1} - \mathbf{u}_\Gamma^n\end{aligned} \tag{13}$$

The Aitken's dynamic parameter is obtained as[37]

$$\omega^n = -\omega^{n-1}\frac{(\Delta\mathbf{u}_\Gamma^n)^T(\Delta\mathbf{u}_\Gamma^{n+1} - \Delta\mathbf{u}_\Gamma^n)}{|\Delta\mathbf{u}_\Gamma^{n+1} - \Delta\mathbf{u}_\Gamma^n|^2} \tag{14}$$

As the information from iterations n and $n-1$ is needed, it has been suggested[37,40] to use the last relaxation parameter from the previous time step for the first iteration in a new time step, upper constrained with a ω_{max} to avoid using a value too large,

$$^{t+\Delta t}\omega^1 = \min(^t\omega^n, \omega_{max}) \tag{15}$$

where $^{t+\Delta t}\omega^1$ is the initial relaxation parameter for the new time step and $^t\omega^n$ is the value of the relaxation parameter in the last iteration of the previous time step .This procedure is simple to implement and provides good results in terms of accuracy and robustness.[34,37,39]

while $t < T$ **do**
  $n \leftarrow 0$;
  Predictor: $\tilde{\mathbf{u}}_\Gamma^n = \mathscr{P}_i(\mathbf{u}_\Gamma^t)$;
  while $n < n_{max}$ **do**
    Fluid solver: $\boldsymbol{\lambda}_{f,\Gamma}^{t+\Delta t}(p_\Gamma, \bar{\bar{\boldsymbol{\tau}}}_\Gamma) = \mathscr{F}(\tilde{\mathbf{u}}_\Gamma^n)$
    Structural solver: $\mathbf{u}_\Gamma^{n+1} = \mathscr{S}^{-1}(-\boldsymbol{\lambda}_{f,\Gamma}^{t+\Delta t})$
    Relaxation: $\tilde{\mathbf{u}}_\Gamma^{n+1} = (1-\omega^n)\tilde{\mathbf{u}}_\Gamma^n + \omega^n\mathbf{u}_\Gamma^{n+1}$
    if $\|\tilde{\mathbf{u}}_\Gamma^{n+1} - \tilde{\mathbf{u}}_\Gamma^n\| < \epsilon$ **then**
      break
    else
      $n \leftarrow n+1$
    end
  end
  $\mathbf{u}_\Gamma^{t+\Delta t} \leftarrow \tilde{\mathbf{u}}_\Gamma^{n+1}$
  $t \leftarrow t + \Delta t$
end

Algorithm 3. Block Gauss-Seidel algorithm with predictor and relaxation parameter

Finally, and particularly for strongly non-linear problems, Newton-Raphson methods to obtain the coupled solution[14,36] have been investigated. They require the computation or estimation of the partial derivatives of the fluid and structural root problems with respect to each domain's own variables, and also with respect the crossed variables.[36] This procedure is computationally expensive, and as a result, based on the root equation derived from Eq. 12, the Interface Newton-Krylov methods have been developed.[34,38] In order to avoid the computation of the exact Jacobian, which is quite time consuming due to non-linearities on the interface,[34] some alternatives have been proposed to compute the matrix-vector product of the Jacobian with an arbitrary vector, as for example finite-difference methods[34,41] or reduced-order models.[38,42] Even though the Newton-Krylov method is expected to have a lesser number of iterations per time step due to its higher order of convergence, the higher cost of each iteration results in comparable overall computational times with the Block Gauss-Seidel method with Aitken's relaxation.[34,37]

II.E. Space coupling

When a partitioned approach is adopted in Fluid-Structure Interaction problems, one also needs to appropriately transfer the coupling conditions defined in II.C between the fluid and structural solvers. Due to the noticeable differences on the physical behavior of both fluid and structure fields, it seems unreasonable to subordinate the discretization of one of the fields to the discretization of the other, particularly if there are local effects on one of them. There is a substantial body of literature to address the problem of coupling two non-matching meshes.[1,13,43–47] Indeed, the interpolation of fields on the interface may compromise

the accuracy of the whole simulation if it is not done appropriately.[44] In general, the information transfer between solvers has to meet strict criteria regarding conservativeness of momentum and energy; at the same time it has to aim at obtaining an efficient solution from the numerical point of view.[1] In this sense, both accuracy and robustness must be achieved in the transfer scheme, which at the same time has to be efficient (maximum accuracy with minimum cost) and simple to implement.[44,45]

It is a common approach in the literature to apply the principle of virtual work[1,44,45,48] to define a conservative transfer scheme. Brown[49] and Farhat[1] have introduced projection methods that apply the conservation of virtual work to the problem of transferring load and deformations in FSI problems on non-matching meshes. By requiring the interpolation method to conserve virtual work across the displacements and forces on the two meshes, the resulting distributions are physically consistent and result in the same integrated forces. Following their work, Equation (16) gives an expression for the virtual work performed by the forces applied to the structure $\mathbf{F}$, moved through a virtual nodal displacement $\delta\mathbf{u}_{\Gamma,s}$.

$$\delta W_E = \mathbf{F}^T \cdot \delta\mathbf{u}_{\Gamma,s} \tag{16}$$

The virtual work must equal the similar expression using the forces of the fluid solution and the virtual displacements of the fluid mesh as shown in Equation (17). For the common case of a finer fluid mesh we have a set of distributed forces $\boldsymbol{\lambda}_f$ including both surface pressure and traction.

$$\delta W_E = \int_{\Gamma,f} (-p\vec{n}_f + \bar{\bar{\boldsymbol{\tau}}}_f \vec{n}_f)^T \cdot \delta\mathbf{u}_{\Gamma,f} dS_f \tag{17}$$

where $\vec{n}_f$ is the unit normal on the fluid side of the problem and S_f the curvilinear coordinate along the fluid interface. Equating Equations (16) and (17):

$$\mathbf{F}^T \cdot \delta\mathbf{u}_{\Gamma,s} = \int_{\Gamma,f} (-p\vec{n}_f + \bar{\bar{\boldsymbol{\tau}}}_f \vec{n}_f)^T \cdot \delta\mathbf{u}_{\Gamma,f} dS_f \tag{18}$$

In the discrete interface, the displacements on the fluid side may be mapped from the displacements on the structural side using a matrix $\mathbf{H}$ that will need to be defined for each problem and method used, thus resulting $\mathbf{u}_f = \mathbf{H}\mathbf{u}_s$. According to the previously described principle of virtual work, the tractions at the structural interface may be mapped from the fluid domain as $\boldsymbol{\lambda}_s = \mathbf{H}^T\boldsymbol{\lambda}_f$. Therefore, it is possible to define a full space-coupling scheme that would meet the criteria of conservation of work just by adequately defining a transformation matrix $\mathbf{H}$. Global conservation of forces can also be achieved just by imposing that the rowsum of $\mathbf{H}$ is equal to one.[45]

Projection methods are based on the idea of orthogonally projecting the information from certain defined points on the source mesh onto the target mesh. Two widely extended projection methods are the node projection method[1] and the quadrature projection method.[43] Projection methods are simple to implement, have been demonstrated to be strictly conservative, and have already been quite successfully used in relevant applications, as for example by Breuer *et al.*[50] analysing an elastic appendix downwind a circular cylinder using LES.

Projection methods may be included within a larger group of interpolation methods to obtain the matrix $\mathbf{H}$ available in the literature: the weighted residual formulations. Jiao and Heath[51] define the problem as one in which the objective is to pass a function $g(\mathbf{x}_d)$ defined at any point $\mathbf{x}_d$ in the donor mesh and obtain a function $h(\mathbf{x}_t)$ defined at any point in the target mesh $\mathbf{x}_t$, in which both $g(\mathbf{x}_d)$ and $h(\mathbf{x}_t)$ are defined as linear combinations of a set of discrete values at the nodes multiplied by a set of shape functions. The objective is to minimize in a certain way the residual $h - g$.[51]

As drawbacks of these methods, Breuer *et al.*[50] point out the occurrence of non-physical distribution of the loads when the structural mesh is finer than the fluid mesh, and Jaiman *et al.*[47,52,53] refer to some problems related with the accuracy and repeated data transfer of these methods. Also, Jiao and Heath[51] carry out an interesting reflection on the conservativeness requirements, as they consider not to be justified enforcing equilibrium over two different discretizations of the same surface. As a result, they propose to enforce conservativeness conditions into an intermediate, sometimes called virtual surface, a concept which has also been addressed by many other authors.[13,14,54]

Another extended family of methods are the Radial Basis Functions (RBF). Radial basis functions have been very successful in various Fluid-Structure Interaction applications,[44,48] also obtaining accurate results in the review carried out by de Boer et al.[45] The method is well described by Beckert and Wendland,[48] and is based on the definition of an interpolation function as

$$g(\mathbf{x}) = \sum_{i=1}^{N} \alpha_i \Phi(\|\mathbf{x} - \mathbf{x}_i\|) + p(\mathbf{x}) \tag{19}$$

where N is the number of *centers*, $\mathbf{x}_i$, distinct from each other, and with a set of associated discrete values g_i, i ranges from 1 to N, $\Phi(\|\mathbf{x}\|)$ is the radial basis function that depend on the method adopted and both the coefficients α_i and the low degree polynomial $p(\mathbf{x})$ are to be determined from the interpolation conditions.[48] One widely extended function in literature relevant to Fluid-Structure Interaction problems is the Thin-Plate Splines (TPS) function, applicable on the interpolation of flexible surfaces,[44] and defined as

$$\Phi_{TPS}(\|\mathbf{x}\|) = \|\mathbf{x}\|^2 \log \|\mathbf{x}\| \tag{20}$$

A similar method is the multiquadric RBF, which uses quadratic basis functions and an user-defined parameter a that controls the shape of the function[44]

$$\Phi_{MQ}(\|\mathbf{x}\|) = \sqrt{\|\mathbf{x}\|^2 + a^2} \tag{21}$$

According to Smith *et al.*[44] and de Boer *et al.*,[45] both of these functions are appropriate for their use with unstructured grids and typically yield accurate results without the need of orthogonal projection or search algorithms. On the other hand, they have shown problems when sharp discontinuities appear in the function that is to be transferred, and also a high computational cost. In order to reduce this cost, it is possible to employ functions with compact support, this is, only a few nodes within a certain radius of the center are affecting the interpolation.[48] One of the most extended compactly supported functions is Wendland three-dimensional C^2 function[55]

$$\Phi_W(\|\mathbf{x}\|) = (1 - \|\mathbf{x}\|/r)^4 (4\|\mathbf{x}\|/r + 1) \qquad \text{for} \qquad \|\mathbf{x}\| < r \tag{22}$$

This function is locally defined by means of the radius r, which is defined a priori, and leaves out of the interpolation any value that is further away from the center than the radius by accepting only positive values on the first term of the equation. A large radius guarantees a better approximation to the solution, whether a small radius can be solved more efficiently. Moreover, the use of a fixed radius guarantees the existence of a solution.[48]

III. Implementation

III.A. Fluid solver

The fluid solver that has been used in this work is the finite volume-based Euler/N-S/RANS solver in SU2. This solver has already been thoroughly described in previous publications by Palacios *et al.*[20,21] and it is not the purpose of this paper to provide a deep revision of its features; the reader may refer to the previously cited articles or to the project website[a]. Nevertheless, in this section a brief description of the solver main features will be carried, explaining the key changes in the code architecture that have been necessary for the implementation of FSI features.

III.A.1. Solution method

For the solution of the fluid equations, Eq. (1), SU2 contains a dual-grid, edge-based discretization that uses vertex-based control volumes,[20,21] as shown in Fig. 3. The semi-discrete form of the fluid problem can be written as

$$\int_{\Omega_i^e} \frac{\partial \mathbf{U}}{\partial t} \mathrm{d}\Omega + \sum_{j \epsilon N(i)} (\tilde{F_{ij}^c} + \tilde{F_{ij}^v}) \Delta S_{ij} = 0 \tag{23}$$

where the numerical convective $\tilde{F_{ij}^c}$ and viscous $\tilde{F_{ij}^v}$ fluxes are projected over the edge ij, ΔS_{ij} is the area of the face associated to that edge, $N(i)$ is the set of nodes who are neighbours to i, and Ω_i is the control volume associated to node i. The summation term in the equation corresponds to the spatial residual, which is computed and stored at the nodes.

[a] http://su2.stanford.edu/

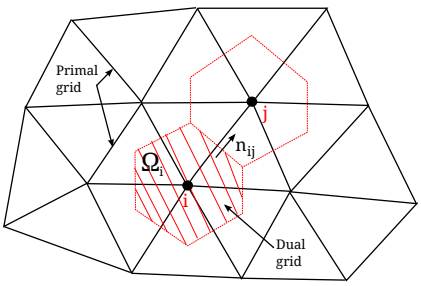

Figure 3. Dual grid discretization

Several upwind and centered methods to compute the convective and viscous terms have been implemented in SU2. Regarding time integration, a dual time-stepping strategy[56] is adopted. The fluid problem is reformulated introducing a fictitious time variable τ that is used to converge a pseudo-steady state problem, resulting in

$$\frac{\partial \mathbf{U}}{\partial \tau} + R^*(\mathbf{U}) = 0 \tag{24}$$

where the modified residual $R^*(\mathbf{U})$ for a 2^{nd}-order in time scheme is

$$R^*(\mathbf{U}) = \frac{3}{2\Delta t}\mathbf{U} + \frac{1}{|\Omega|^{n+1}}\left(R(\mathbf{U}) - \frac{2}{\Delta t}\mathbf{U}^n\,|\Omega|^n + \frac{1}{2\Delta t}\mathbf{U}^{n-1}\,|\Omega|^{n-1}\right) \tag{25}$$

being Δt the physical time step and $R(\mathbf{U})$ the residual of the original equation.

III.A.2. Code structure

The code structure has been previously defined by Palacios *et. al*,[20] but it has been modified in this work in order to more effectively account for multi-zone multidisciplinary problems. This is described in Fig. 4. Two new layers of abstraction have been introduced in the main core, namely the *CDriver* and *CIteration* classes, in order to increase the modularity of the solver and to ease the coupling of different features.

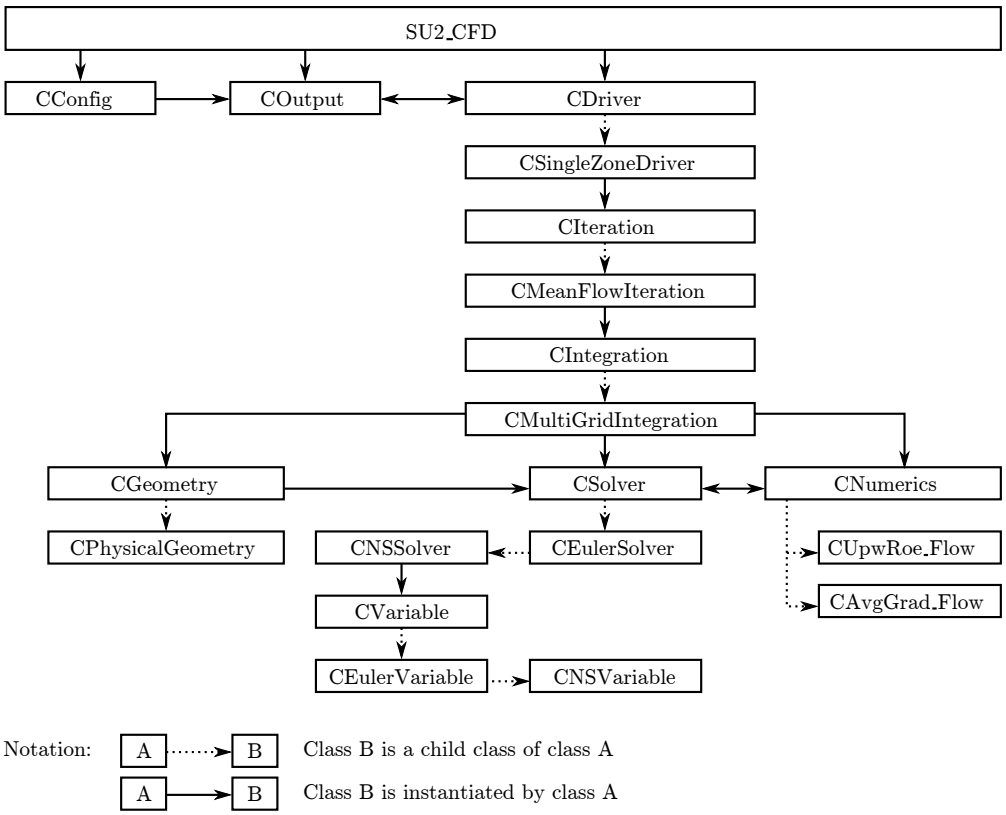

Figure 4. Class hierarchy for solving a Navier-Stokes problems.

From bottom to top, the class *CIteration* accounts for the different stages of the solution process within one time step. In particular, it provides support for the pre- and post-processing of the solver, the iteration itself and the solution update once convergence has been reached. The modularity of this approach permits to combine different solvers using the upper-level class *CDriver*. For a single zone, the child class *CSingleZoneDriver* is in charge of performing the operations of *CIteration* in the appropriate order; the full potential of this class will be further described in section III.C.1. With the objective of completeness, the

full list of the child classes available at the time of writing for this two new classes is given in Fig. 5. The new layers of abstraction are designed so that one can more easily couple multiple physics within a flexible framework, including new multi-physics implementations not previously envisioned by the authors.

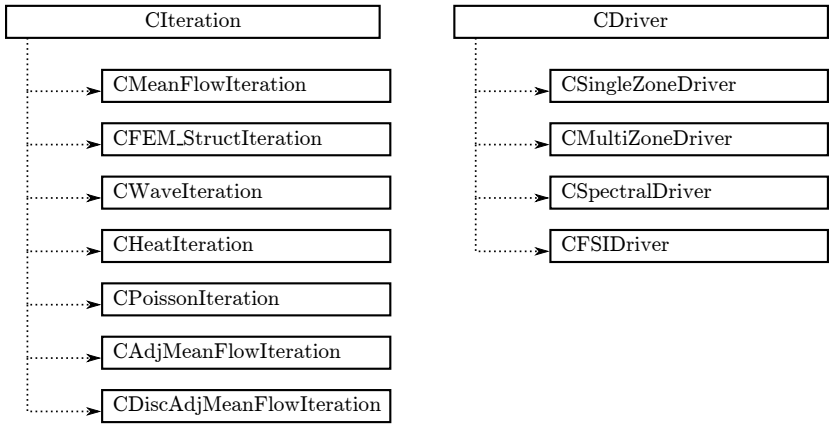

Figure 5. List of child classes for the CIteration and CDriver classes.

III.B. Structural solver

The structural solver has been fully recast in order to improve its flexibility and allow for the solution of more complex, geometrical and material non-linear problems. In order to do so, a whole new infrastructure has been built and developed in terms of a new set of classes that will be described in this section. This new scheme will ease further improvements to the suite, such as the use of higher-order Finite Elements, or the employment of more complex material models than those described here, simply by adding new child classes to the current structure.

III.B.1. Solution method

The current implementation allows for static and dynamic structural analysis using both a linear elastic setting, and a large-deformations geometrically non-linear problem with hyperelastic, compressible Neo-Hookean material model.

In a linear setting, and assuming no structural damping, Eq. (5) may be discretized in space using the Finite Element Method. Given that the body is subject to a set of externally applied forces $\mathbf{F}_e$, the structural response will be calculated by imposing equilibrium at the nodes using the principle of virtual work, subject to boundary and compatibility conditions. The resulting expression for linear elasticity may be written as the product of a mass matrix $\mathbf{M}$ and a stiffness matrix $\mathbf{K}$, multiplying respectively the acceleration and displacement terms of the solution[57]

$$\mathbf{M}\ddot{\mathbf{u}} + \mathbf{K}\mathbf{u} = \mathbf{F}_e \tag{26}$$

In a non-linear setting, however, the nature of the problem requires the linearization of the principle of virtual work. The problem may now be written in an Updated Lagrangian implicit Newton-Raphson formulation as[57,58]

$$\begin{aligned} \mathbf{M}^{t+\Delta t}\ddot{\mathbf{u}} + {}^{t+\Delta t}\mathbf{K}\Delta\mathbf{u}^n &= {}^{t+\Delta t}\mathbf{F}_e - {}^{t+\Delta t}\mathbf{T}^{n-1} \\ {}^{t+\Delta t}\mathbf{u}^n &= {}^{t+\Delta t}\mathbf{u}^{n-1} + \Delta\mathbf{u}^n \end{aligned} \tag{27}$$

where the stiffness matrix $\mathbf{K} = \mathbf{K}_c + \mathbf{K}_\sigma$ accounts for the constitutive and stress terms of the equations and $\mathbf{T}$ is the vector of internal equivalent nodal forces. For nodes a and b within an element e, the constitutive and stress components of the tangent matrix, the internal nodal forces vector, and the mass matrix, may be written as[57,58]

$$
\begin{aligned}
\mathbf{K}^e_{c,ab} &= \int_{\Omega^e_s} \mathbf{B}^{e^T}_a \mathbf{D}^e \mathbf{B}^e_b d\Omega^e_s \\
\mathbf{K}^e_{\sigma,ab} &= \int_{\Omega^e_s} (\nabla \mathbf{N}^e_a \cdot \boldsymbol{\sigma}^e \nabla \mathbf{N}^e_b) \mathbf{I} \mathrm{d}\Omega^e_s \\
\mathbf{M}^e_{ab} &= \int_{\Omega^e_s} \rho^e_s \mathbf{N}^{e^T}_a \mathbf{N}^e_b \mathrm{d}\Omega^e_s \\
\mathbf{T}^e_a &= \int_{\Omega^e_s} \boldsymbol{\sigma}^e \nabla \mathbf{N}^e_a \mathrm{d}\Omega^e_s
\end{aligned}
\tag{28}
$$

In terms of material modelling, a linear elastic formulation has been implemented. Three-dimensional and two-dimensional analysis using either plane stress and plane strain assumptions are allowed. For non-linear applications, a compressible neo-Hookean non-linear material model has been implemented, which has the following expression for its free energy function:[58]

$$
\Psi = \frac{\mu}{2}(\mathrm{tr}(\mathbf{b}) - 3) - \mu \ln J + \frac{\lambda}{2}(\ln J)^2 \tag{29}
$$

With regards to the time integration, the Newmark[59] and the Generalized-α[60] integration methods have been implemented in SU2. Both methods rely on the approximations

$$
\begin{aligned}
{}^{t+\Delta t}\mathbf{u} &= {}^{t}\mathbf{u} + \dot{\mathbf{u}}\Delta t + [(\frac{1}{2} - \beta)^t \ddot{\mathbf{u}} + \beta^{t+\Delta t}\ddot{\mathbf{u}}]\Delta t^2 \\
{}^{t+\Delta t}\dot{\mathbf{u}} &= {}^{t}\dot{\mathbf{u}} + [(1-\gamma)^t \ddot{\mathbf{u}} + \gamma^{t+\Delta t}\ddot{\mathbf{u}}]\Delta t
\end{aligned}
\tag{30}
$$

The Newmark method imposes equilibrium at the end of the time step according to Eq. (27), while the Generalized-α method introduces the parameters α_m and α_f $(0 < \alpha_f, \alpha_m < 1)$ and imposes equilibrium at an intermediate point within the time step, as

$$
\begin{aligned}
\mathbf{M}^{t+\Delta t-\alpha_m}\ddot{\mathbf{u}} + {}^{t+\Delta t-\alpha_f}\mathbf{K}\Delta\mathbf{u}^n &= {}^{t+\Delta t-\alpha_f}\mathbf{F}_e - {}^{t+\Delta t-\alpha_f}\mathbf{T}^{n-1} \\
{}^{t+\Delta t-\alpha_f}\mathbf{u}^n &= {}^{t+\Delta t-\alpha_f}\mathbf{u}^{n-1} + \Delta\mathbf{u}^n
\end{aligned}
\tag{31}
$$

III.B.2. Code structure

A Finite-Element Method based, non-linear structural solver has been implemented in SU2, following the same philosophy of modularity as the original fluid solver. This flexible structure of the code will allow for a sustainable growth of the code, as new features may be added to address more complex and specialized problems just by developing and expanding the capabilities. The main modifications in the code affect the *CSolver* and *CNumerics* classes, as shown in Fig. 6, and will be thoroughly described in this section.

With regards to the *CSolver* class, the original CFD code defines an object pertaining to the class *CVariable* for each point in the mesh. The child class of *CVariable* used depends of the physics of the problem, and it is responsible for storing the variables of the problem at the node level. Such structure has been proven to be very adequate for the solution of the fluid problem by means of a dual-grid, edge based Finite Volume integration of the Navier-Stokes equations. The vertex structure has been maintained in the structural solver with the definition of the child class *CFEM_ElasVariable*, as the Finite Element method computes the solution of the structural problem at the nodes of the elements. As a result, the displacements $\mathbf{u}$, obtained from the solution of Eqs. (26) and (27), as well as the velocities $\dot{\mathbf{u}}$ and accelerations $\ddot{\mathbf{u}}$, are stored at the nodes.

The discretization of the continuum using the Finite Element method requires, however, to consider the element also as a basic entity over which the solver will loop and compute the relevant magnitudes. In order to do so, a new *CElement* class has been defined, which hosts the common properties of the FEM structure, and aims for an improved modularity of FE based solvers in SU2. One child class of *CElement* is defined for each relevant kind of element that may be used in SU2. The current implementation is limited to linear, first order elements: 3- and 4-node elements for two-dimensional problems, and 4- and 8-node elements for three-dimensional problems. This list can be extended to include higher-order elements, due to

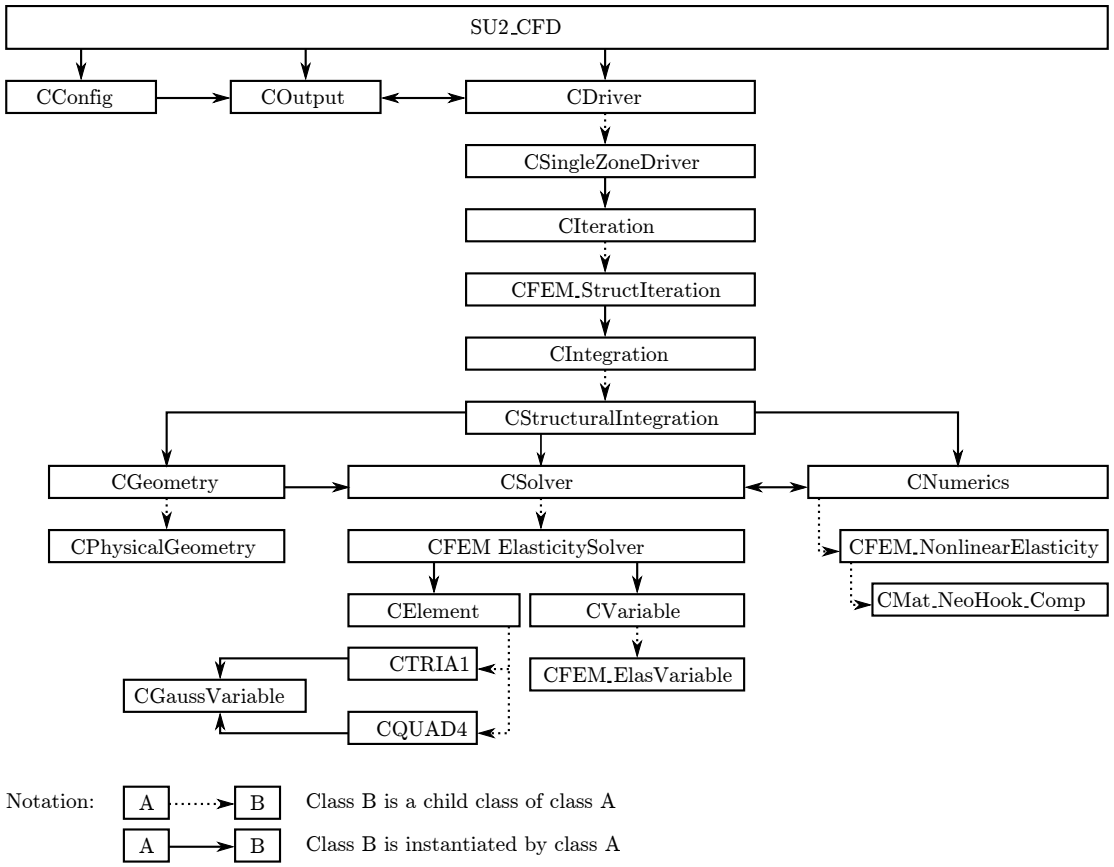

Figure 6. Class hierarchy for solving a two-dimensional, non-linear structural problem.

the flexibility of the parent class *CElement*, not only for structural problems but also for fluid analysis or any other problems not previously envisioned by the authors. The full list available at the time of writing is shown in Fig. 7.

The number that accompanies the name of the element in Fig. 7 defines the number of Gaussian Points which each element uses for a full integration in its domain and to its predefined order. For non-linear structural analysis, several relevant magnitudes such as the deformation gradient $\mathbf{F}$, the Cauchy stress tensor $\boldsymbol{\sigma}$ or the constitutive matrix $\mathbf{D}$ are computed at the Gaussian Points in order to perform Gaussian integration. The same happens with the shape functions $\mathbf{N}$ and their gradients $\nabla\mathbf{N}$. Therefore, an auxiliary class CGaussVariable has been defined, that temporarily stores the value of these magnitudes until the full element has been integrated. This class is common to all elements.

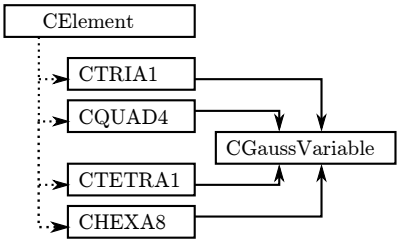

Figure 7. List of child classes for the CElement class.

With regards to the *CNumerics* class, two levels of inheritance have been defined and are directly related to the two types of non-linearity that may be encountered in structural analysis. At the first level, the child classes *CFEM_LinearElasticity* and *CFEM_NonlinearElasticity* have been defined (Fig. 8), which relate to the geometrical non-linearity of the structural problem. These two classes share common properties through a parent class *CFEM_Elasticity*, although the differences between both approaches justify their separation into

two different child classes. These classes are responsible for computing, at the element level, the constitutive and stress terms of the tangent matrix, the mass matrix or any other relevant term for the left or right hand side of Eqs. (26) and (27). The final assembly and imposition of boundary conditions will then be done by *CFEM_ElasticitySolver*.

In order to account for material non-linearities, a second level of inheritance has been defined (Fig. 9) under the class *CFEM_NonlinearElasticity*. These child classes contain the equations that define the material model to be employed and have the common interface with the geometrical part of the problem in the computation of the constitutive matrix $\mathbf{D}$ and the Cauchy stress tensor $\boldsymbol{\sigma}$. The current implementation in SU2 includes a Neo-Hookean compressible hyperelastic material model, and more models will be incorporated due to the modular structure of the code.

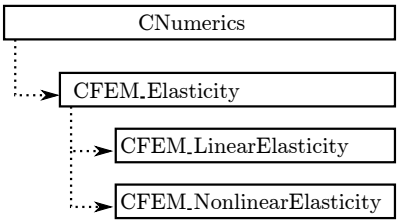

Figure 8. Child class structure for the definition of geometrical non-linearities.

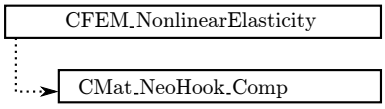

Figure 9. Child class structure for the definition of material non-linearities.

III.C. Coupled solver

The high computational cost per iteration of Newton-Raphson methods, together with a simpler and more modular implementation, has led to the development in this work of a Block Gauss-Seidel method with Aitken's relaxation for time-accurate coupling. With regards to spatial coupling, the code is being built to accommodate both RBF and projection methods, for their application in problems with non-matching discretizations. The structure of the code will be further described in the following sections.

III.C.1. Code structure for time coupling

In order to tackle the solution of problems with two or more physical domains, it was found necessary to define two new classes, *CDriver* and *CIteration*. This has already been explained in section III.A.2, but the full potential of the class *CDriver* may be seen in this section. In the context of multi-physics problems, this will be the class responsible for driving the simulation and determining the sequence at which the iterations of the different solvers are run. Using this abstraction, a whole set of completely independent solvers may be built by different and specialized teams, and then combined together for multi-disciplinary studies.

The solution of each problem is obtained independently using the appropriate solver on each case. The BGS method requires, however, that the solutions need to be communicated through a common interface in order to enforce equilibrium and compatibility conditions at the end of each time step. It is important to note that, for parallel simulations, this communication has to be carefully performed, as the decomposition of either one of the physical domains involved in the calculations does not necessarily have to be compliant with the rest. As a result, an independent parent class *CTransfer* has been built, which transfers the information between two independently discretized and decomposed domains using the adequate MPI instructions.

At the same time, the parent class *CTransfer* has a set of child classes which account for the physics of the transfer. For example, in a Fluid-Structure Interaction problem, the fluid tractions applied over the interface will be transferred from the fluid domain to the structural domain, while in the opposite direction the relevant magnitudes are the structural displacements along the boundary. This separation in parent (geometrical) and child (physical) classes allows for the code to grow independently in performance and features. This means that new child classes may be defined in the future for different kinds of multi-zone problems without interfering with the routines that define the parallel transfer of the information. In the same way, these routines may be improved without modifying the physics behind the solvers. This structure is further described in Fig. 10.

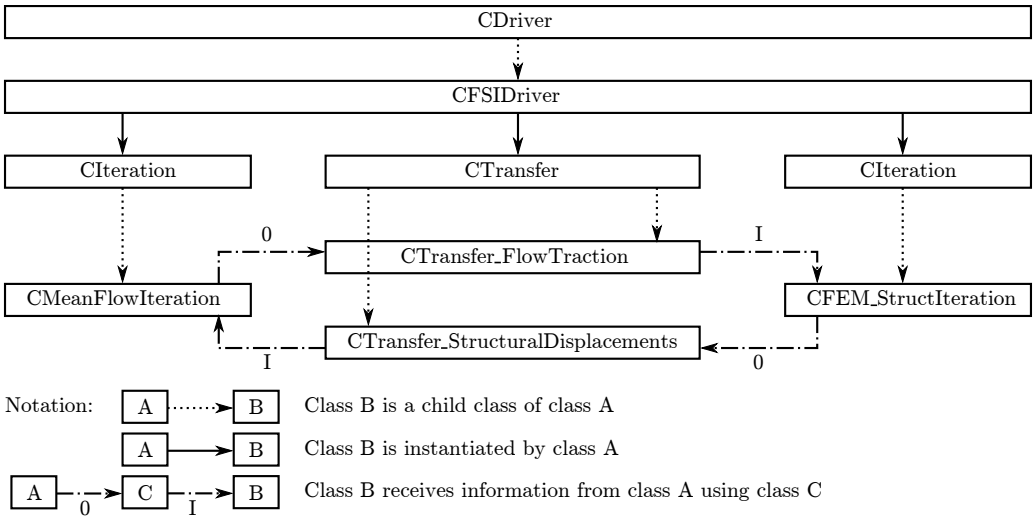

Figure 10. Class structure for the information transfer between two solvers

III.C.2. Code structure for spatial coupling

The interpolation class *CInterpolate* has been built independently of the transfer *CTransfer* class, in order to maintain the modularity of the code. The class relies on the dual grid structure described by Palacios *et al.*,[20] by storing the information of the donor points and the relevant terms of the transformation matrix **H** at the target vertices (Fig. 11).

During the interpolation process, each vertex will receive the physical information from the relevant child class of *CTransfer* and use it appropriately in accordance with the interpolation procedure of choice. Each interpolation procedure constitutes a child class of the parent *CInterpolate* class. The list of child classes available at the time of writing is shown in Fig. 12. Preliminary studies using Nearest-Neighbor and Isoparametric interpolation methods confirm the validity of the proposed structure and encourage the development of some of the methods developed in section II.E. In particular, the consistent and conservative interpolation method proposed by Brown[49] has been already implemented and is further developed in the next section.

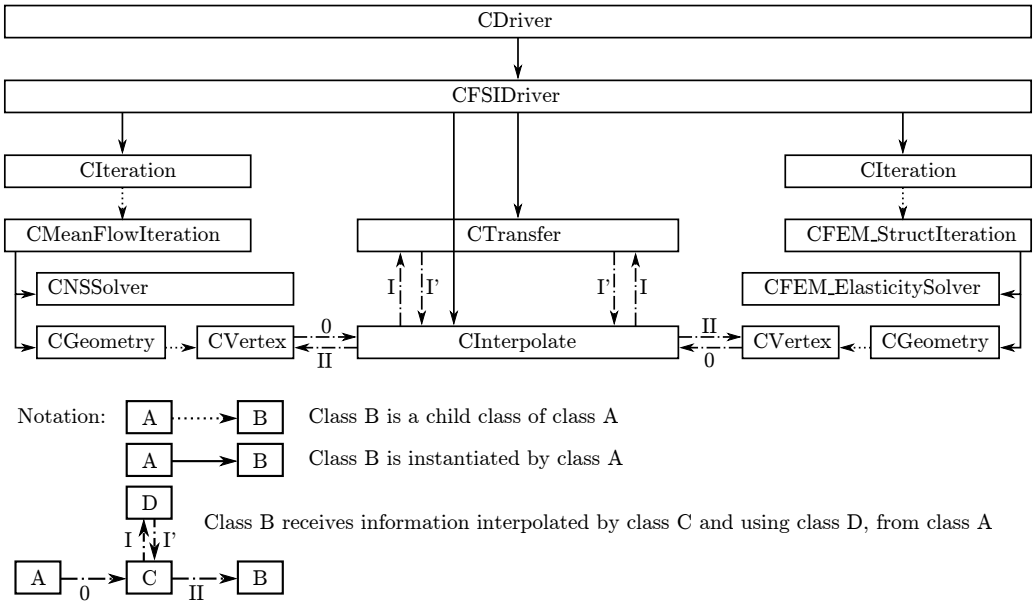

Figure 11. Class structure for the interpolation of information between two discretizations

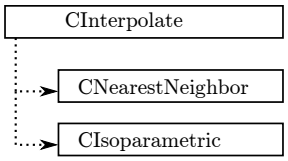

Figure 12. Child class structure for the implementation of interpolation methods

III.C.3. Consistent and conservative interpolation method

Interpolation schemes with non matching meshes and external structural solvers have already been successfully demonstrated in SU2,[61] and a consistent and conservative method has been implemented natively in the context of this work to assess the validity of the code structure, following the work of Brown.[49]

According to Brown,[49] it is possible to use a set of assumed displacement functions to interpolate the displacement of the structure in between the mesh nodes, which gives a set of linear functions of the nodal displacements $\mathbf{u}_s$ for the displacement at any point in a finite element. By linking each node in the fluid mesh by a rigid rod to the nearest node on the structure mesh we can use the displacement interpolated within a single finite element and relate the displacements for points that are not exactly coincident with the plane of the finite element. In Equation (32), $\mathbf{X}$ are the points on the fluid mesh and $\mathbf{x}$ are the points on the structure mesh which are translated $u(\cdot)$ and rotated $u_\theta(\cdot)$.

Relating the displacement on the finite element to the displacement of the node on the fluid mesh:

$$\begin{aligned} \mu(\mathbf{X}) &= u(\mathbf{x}) - (\mathbf{X} - \mathbf{x}) \times u_\theta(\mathbf{x}) \\ \mu(\mathbf{X})_\theta &= u_\theta(\mathbf{x}) \end{aligned} \tag{32}$$

Introducing an assumed interpolation between the displacement on the finite element u to the displacement of the finite element nodes $\mathbf{q}$:

$$\mathbf{u}(\mathbf{x}) = \left[n_x(\mathbf{x}) n_y(\mathbf{x}) n_z(\mathbf{x})\right]^T \cdot \mathbf{q} = \boldsymbol{\eta}(\mathbf{x})^T \cdot \mathbf{q} \tag{33}$$

Combining Equations (32) and (33), using the matrix form of the cross product which is expanded in Equation (35).

$$\begin{aligned} \mathbf{u}(\mathbf{x}) &= \left[n_x(\mathbf{x}) n_y(\mathbf{x}) n_z(\mathbf{x})\right]^T \cdot \mathbf{q} = \boldsymbol{\eta}(\mathbf{x})^T \cdot \mathbf{q} \\ \mu &= \boldsymbol{\eta}(\mathbf{x})^T \cdot \mathbf{q} - [\mathbf{X} - \mathbf{x}] \cdot \boldsymbol{\eta}_\theta(\mathbf{x})^T \cdot \mathbf{q} \\ \mu_\theta(\mathbf{X}) &= \boldsymbol{\eta}_\theta(\mathbf{x})^T \cdot \mathbf{q} \end{aligned} \tag{34}$$

$$[\mathbf{X} - \mathbf{x}] = \begin{bmatrix} 0 & (x_3 - X_3) & (X_2 - x_2) \\ (X_3 - x_3) & 0 & (x_1 - X_1) \\ (x_2 - X_2) & (X_1 - x_1) & 0 \end{bmatrix} \tag{35}$$

Using:

$$\begin{aligned} \mathbf{H}(\mathbf{X}) &= \boldsymbol{\eta}(\mathbf{x})^T - [\mathbf{X} - \mathbf{x}] \cdot \boldsymbol{\eta}_\theta(\mathbf{x})^T \\ \mathbf{H}_\theta(\mathbf{X}) &= \boldsymbol{\eta}_\theta(\mathbf{x})^T \end{aligned} \tag{36}$$

we now have extrapolation matrices between the respective meshes.

$$\begin{aligned} \mathbf{F}^T \cdot \delta\mathbf{q} &= \int \mathbf{p}^T \cdot \mathbf{H}^T \delta\mathbf{q} \, dS \\ \mathbf{F}^T &= \int \mathbf{p}^T \cdot \mathbf{H}_\theta^T \, dS \end{aligned} \tag{37}$$

It only remains to find the values for the interpolation matrix $\mathbf{H}^T$, which can be found using isoparametric interpolation functions. With these functions, the value at a point on the aerodynamic mesh can be expressed

as a weighted sum of the values at the nodes of a single element on the structural mesh. Since only the weight values are required, the isoparametric coefficients are not explicitly required.

$$\mu = \begin{bmatrix} (1-r)(1-s) \\ r(1-s) \\ rs \\ (1-r)s \end{bmatrix} \cdot \mathbf{q} = \boldsymbol{\eta}(\mathbf{x})^T \cdot \mathbf{q} \tag{38}$$

The values in $\boldsymbol{\eta}(\mathbf{x})$ can be found by using the coordinates of the points.

$$\begin{bmatrix} 1 \\ \mathbf{x} \end{bmatrix} = \begin{bmatrix} 1 & 1 & ... & 1 \\ \mathbf{x}_1 & \mathbf{x}_2 & ... & \mathbf{x}_n \end{bmatrix} \boldsymbol{\eta}(\mathbf{x})^T \tag{39}$$

For meshes where the points of the aerodynamic and structural meshes are coincident, the coefficients for the interpolation matrix are simply 1 at the matching node and 0 elsewhere. This interpolator is generic and accounts for displacement and rotation degrees of freedom (DOFs). For the solid FEM developments in this work the rotations are neglected as only displacements are considered at the nodes.

III.D. Mesh morpher

An adequate deformation of the fluid mesh is critically important for the final accuracy of the solution and for the computational time involved in the calculations. In this work, the mesh will be deformed using a pseudo-structural approach[62] that will be briefly described in this section.

III.D.1. Solution method

Given a certain displacement vector on the interface $\mathbf{u}_\Gamma$, it is necessary to update the nodes of the whole domain, $\mathbf{u}_\Omega$, in a way that does not compromise the quality of the mesh. The mesh movement problem in SU2 is treated as a linear-elasticity problem $\mathbf{K}^m\mathbf{u}_\Omega = \mathbf{f}$, in which the boundary conditions determine the displacements of the inner nodes. The interface displacements are set to be the structural displacements computed, $\mathbf{u}_{\Gamma,i} = \mathbf{u}_{\Gamma,s}$, while the outer boundaries are set to be static along the problem, $\mathbf{u}_{\Gamma,fext} = \mathbf{0}$. In order to prevent the smaller elements from having negative areas, the stiffness is set cell-dependent, as an inverse function of the element's area or volume, $E^e = \min(\Omega^j)/\Omega^e$. The Lamé constants are finally determined as $\mu^e = E^e$ and $\lambda^e = -E^e$,[62] thus completely defining the problem.

III.D.2. Code structure

The structure of the mesh morpher is independent from the particular solver that need to use it, and only depends on the particular discretization of the physical domain under study, as outlined in Fig. 13.

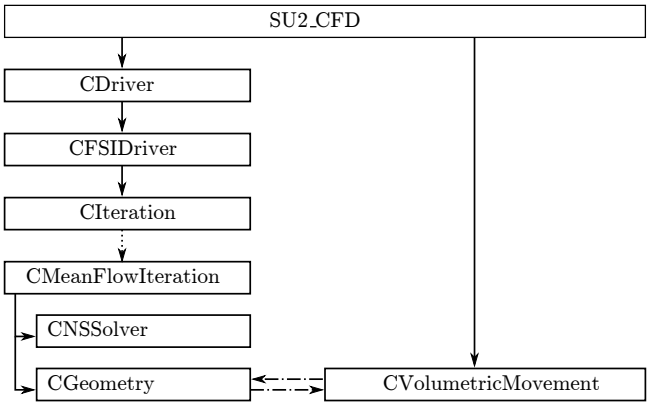

Figure 13. Class structure for the mesh morphing of the fluid discretization

IV. Numerical Results & Discussion

The current implementation of the coupled solver allows both for a loosely-coupled, Conventional Serial Staggered (CSS) time coupling and for a strongly-coupled, Block Gauss-Seidel method with relaxation, using a fixed or a dynamic Aitken's parameter, as explained in section II.D. The spatial coupling will be limited here to a common discretization of the interface for fluid and structure. The structural solver is able to run either linear analysis or non-linear analysis both in terms of geometry and material properties. In order to address the verification and validation of the fluid solver with an ALE formulation, the reader may refer to section V.A.5 in the paper by Palacios *et al.*[20] To investigate the implementation of the FSI problem, we will study the behavior of a flexible beam attached on the downwind side of a rigid square, a problem that has been used extensively as benchmark for Fluid-Structure Interaction applications.[14,18,23,26,39,41,63]

IV.A. Problem description

The geometrical and physical description of the case is shown in Fig. 14 and Table 1. The problem is computed in 2D, and consists of a square cylinder immersed in a low-Reynolds number flow. The cylinder sheds vortices, which generate areas of low-pressure on its wake. A flexible cantilever is attached on the downwind side of the square, and receives an alternated force generated by the vortex street, therefore suffering from vortex-induced vibrations. For a linear model, the first natural bending mode of the structure corresponds to 3.03 Hz. The boundary conditions are set to inlet on the upwind side, outlet on the downwind side, and slip walls on the upper and lower boundaries. The square and the appendix are set to no-slip walls.

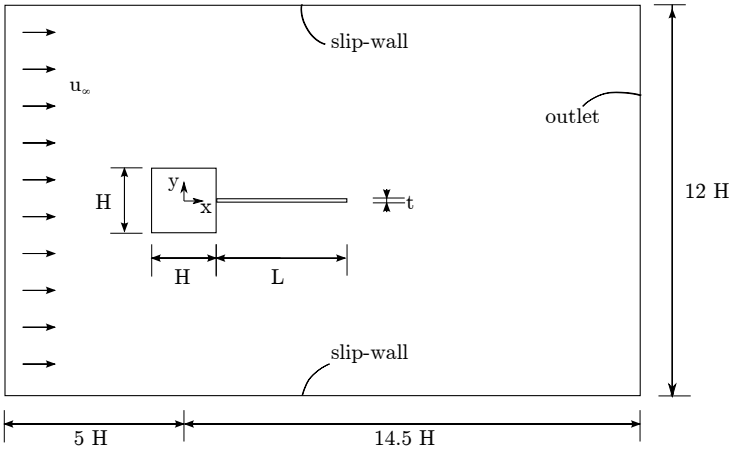

Figure 14. Fluid-Structure Interaction test case (not to scale)

Table 1. Problem definition

Geometry					
H	1	cm			
L	4	cm			
t	0.06	cm			
Fluid			**Structure**		
u_∞	0.513	m/s	E	$2.5 \cdot 10^5$	Pa
ρ_f	1.18	kg/m^3	ρ_s	100	kg/m^3
μ_f	$1.82 \cdot 10^{-5}$	kg/m·s	ν	0.35	
Re	332				
Ma	0.2				

This problem was originally proposed in 1998 by Wall and Ramm,[63] and has since then been used as benchmark for numerous FSI implementations. Two parameters that are extensively used in the literature

as a validation criterion are the frequency and maximum amplitude of the vertical displacements at the tip of the cantilever. The reported frequencies range normally from 3.0 to 3.2 Hz, while the tip displacements range from 1.0 to 1.35 cm. A third criterion will be used in this paper, which is the modulation of the response by higher frequency effects. Some authors, as for example Dettmer and Perić[14] or Froehle and Persson,[18] have presented time histories that show the presence of a second mode of vibration. As Dettmer and Perić already highlighted and as it will be seen in this paper, convergence analysis show the rather complex nature of the dynamics of this configuration.

IV.B. Convergence study

For this paper, three different meshes have been generated using a dual-grid FV discretization. They will be named *coarse*, *fine* and *finest*. They combine triangular elements and boundary layer refinement to be able to capture the separation due to the bluff bodies at the tested Reynolds number. The cantilever is discretized using a fine, 1128-quadrilateral, linear FE mesh, using 6 elements in the thickness. The meshes were generated using the open-source code Gmsh,[64] and for the region closer to the body they are shown in Fig. 15. The properties of the meshes are compared in table 2.

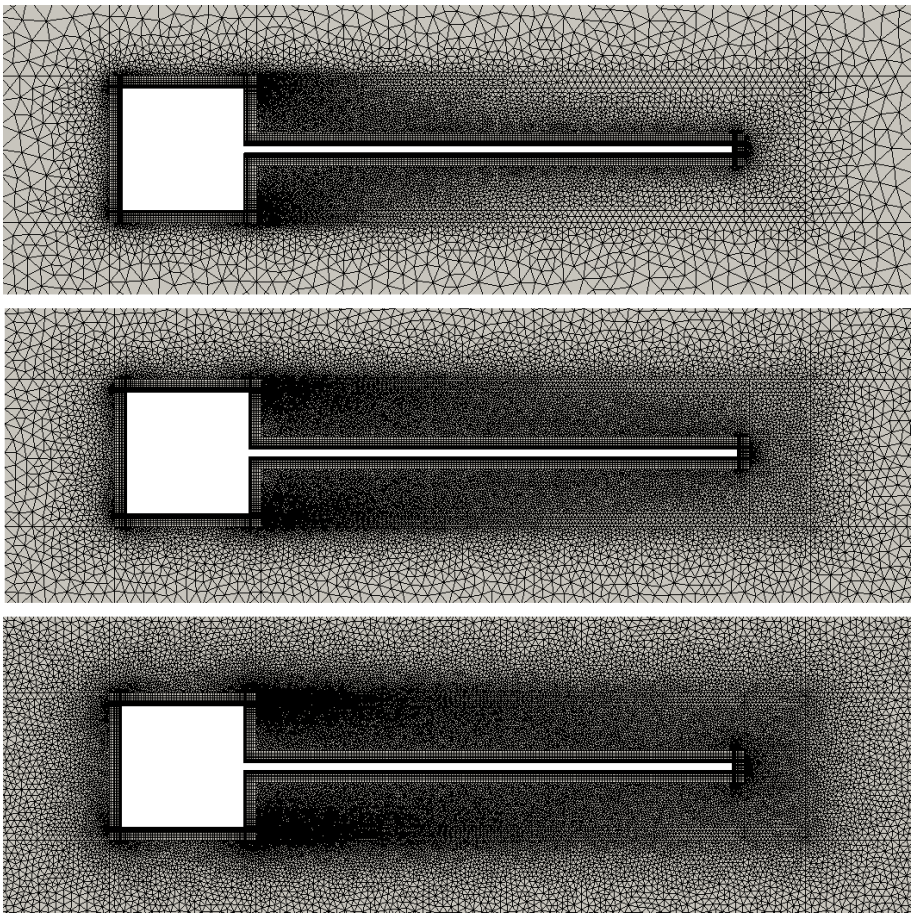

Figure 15. Fluid discretizations: *coarse* (top), *fine* (center) and *finest* (bottom) meshes for the FSI benchmark.

Table 2. Mesh refinement for convergence study

Mesh	Fluid nodes	Structural elements
Coarse	18778	
Fine	27216	1128
Finest	38988	

The coupled problem will be solved in all cases using a Block-Gauss-Seidel (BGS) approach with dynamic Aitken's relaxation. The convergence criteria on the interface is set to 1/1000 of the cantilever thickness, which generally requires between 4 to 5 iterations to converge. A staggered approach was found to diverge for a time step $\Delta t = 0.0075$ s. Two subiterations of the BGS method, however, were enough to maintain the stability of the simulation for all the tested cases, which matches the reported by Wood *et al.*[23] The structure is integrated using a Newmark time integration procedure as explained in section III.B.1, incorporating a 2% numerical damping in order to prevent the divergence of the solver due to high frequency structural effects. The solver is started from a slightly perturbed, symmetric fluid state, previously computed with a static beam in order to avoid non-physical transient effects due to the initialization of the fluid solver. In terms of time accuracy, all three domain discretizations have been run using two different time discretizations, with $\Delta t = 0.0075$ s as the reference time step and $\Delta t = 0.005$ s for an improved solution. The time histories of the vertical tip displacements and the Fourier transform analysis are shown in Fig. 16 for all three discretizations and for the two time steps considered.

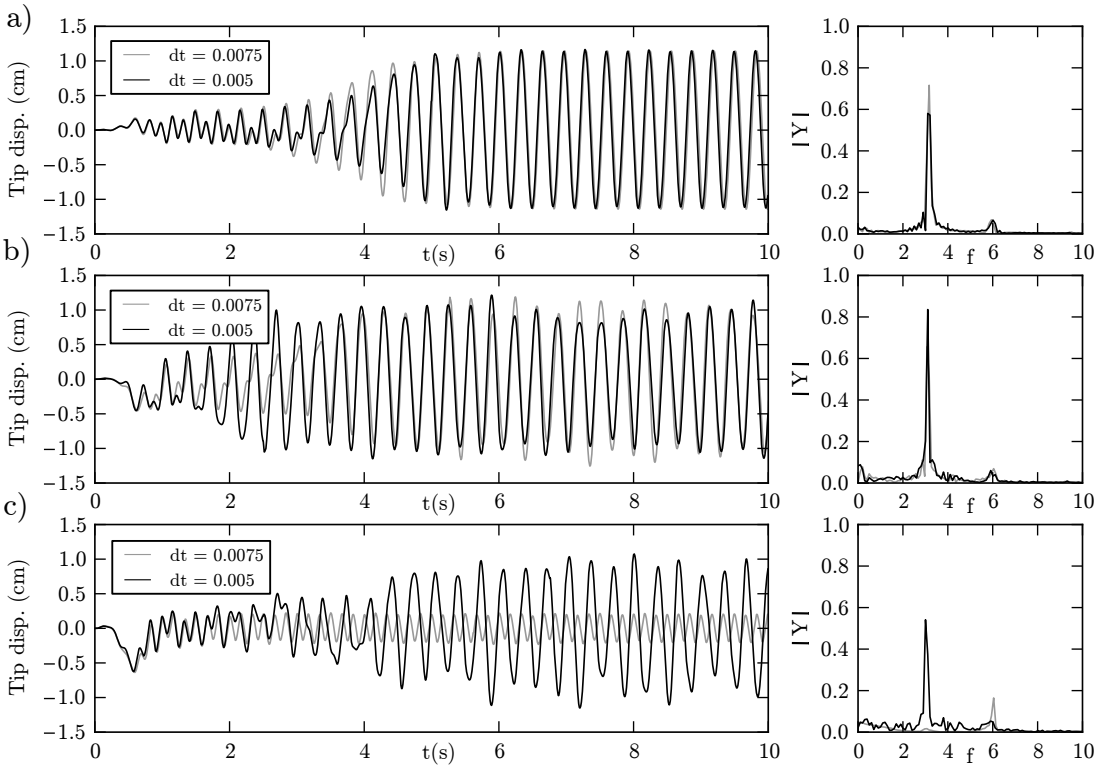

Figure 16. Time histories of the vertical displacements at the tip of the cantilever and FFT plots, for the a) *coarse*, b) *fine* and c) *finest* fluid discretizations, and the two time steps considered, $\Delta t = 0.0075$ s and $\Delta t = 0.005$ s

Firstly, it may be observed in Fig. 16,a) that the *coarse* mesh has been converged with the time step. The time histories for $\Delta t = 0.0075$ s and $\Delta t = 0.005$ s almost overlap. The frequency and amplitude measured match quite well for both cases, and no higher frequency effects are clearly appreciated in any of the time discretizations. It may be observed that the beam starts to vibrate with a higher frequency, which according to the FFT plot is estimated to be around 6 Hz. After 5 seconds of simulation, the cantilever has reached a stationary state of vibration with an average frequency $\bar{f}$=3.15 Hz, with a maximum amplitude d_{max}=1.15 cm. These results agree well with the results published in the open literature. It is noted, however, that the vibration only occurs at one frequency once the stationary state has been reached; no higher frequency effects are observed.

However, for the *fine* discretization, this is no longer true, see Fig. 16,b). In this case, a higher frequency wave clearly modulates the amplitude of the vibration. This behavior matches the observations of Dettmer and Perić (2006)[14] regarding the appearance of high frequency effects for dense spatial discretizations. For $\Delta t = 0.0075$ s, the mean frequency measured is calculated to be $\bar{f} = 3.10$ Hz, ranging from 3.04 to 3.19 Hz, and with a maximum amplitude $d_{max} = 1.25$ cm. For $\Delta t = 0.005$ s, the mean frequency measured is $\bar{f} = 3.11$ Hz, ranging from 2.96 to 3.22 Hz, and the maximum amplitude $d_{max} = 1.21$ cm. Two peaks are

observed at the FFT plot; the first peak corresponds with the vibration of the appendix, while the second corresponds to 6 Hz of frequency. The stationary state reached is equivalent for both time steps, so the solution is fully converged. A contour plot of the pressure field and the structural displacements is presented in Fig. 17 for both discretizations. It may be observed that some vortical structures are pointed out, as they are remarkably more defined for the *fine* discretization (Fig. 17, b) respect to the coarse discretization (Fig. 17, a).

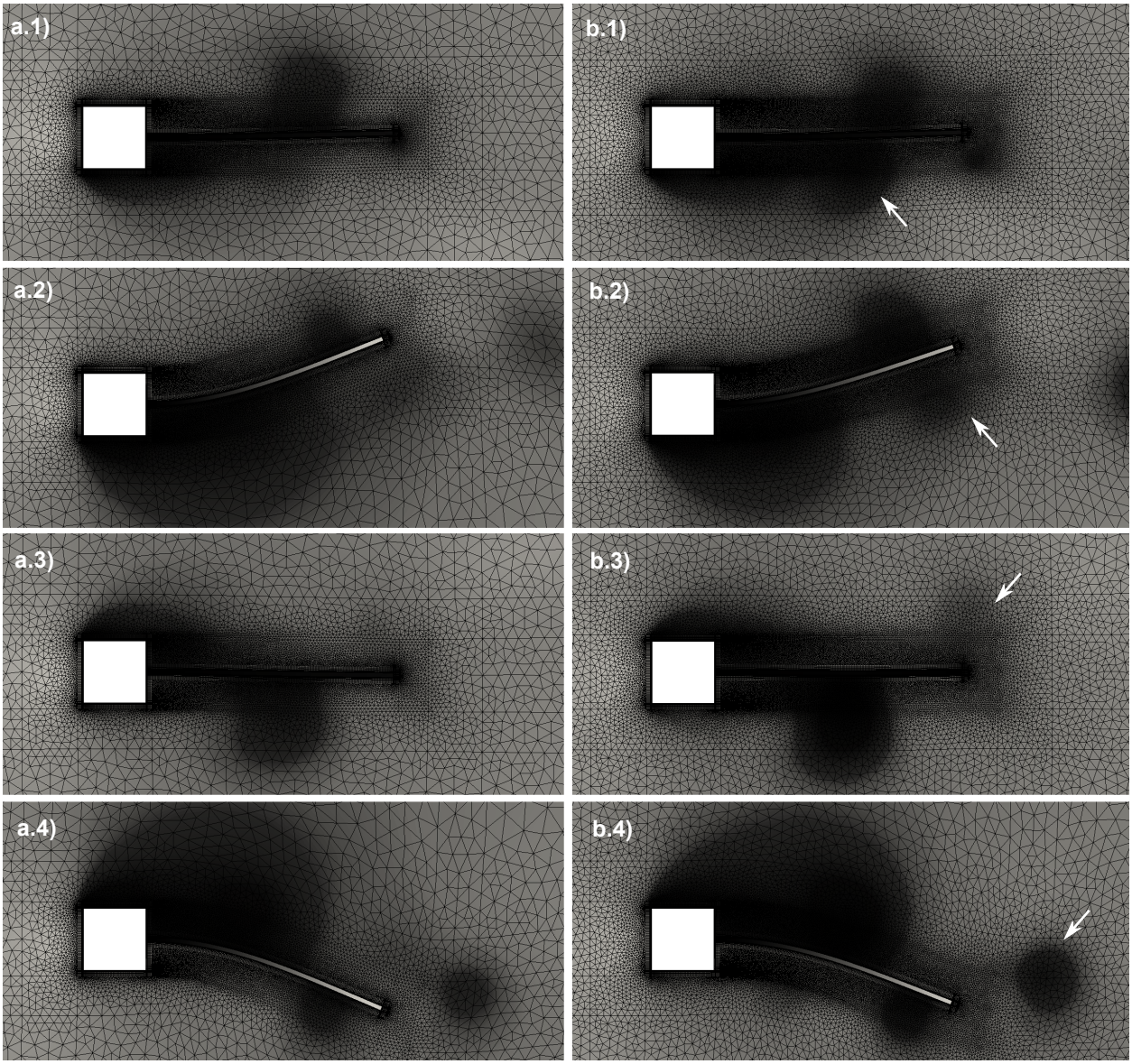

Figure 17. Pressure contours and structural displacements for a cycle of vibration for the *coarse* mesh (a) and for the *fine* mesh (b). T=0 (1), T=π/2 (2), T= π (3), T=3π/2 (4). The arrow in (b) points out some vortical structures that are damped out by the coarser discretization.

The behavior of the coupled problem changes significantly for the most refined, *finest* discretization. In particular, the problem converges to two different solutions depending on the time step. A larger time step, $\Delta t = 0.0075$ s, converges to a solution in which the cantilever vibrates with an average frequency $\bar{f} = 6.0$ Hz, which ranges from 5.7 to 6.27 Hz, and a maximum amplitude $d_{max} = 0.23$ cm. This behavior is completely different from the general behavior of the coupled problem reported in the literature, and also from the results obtained in this work with different discretizations but the same general settings. Interestingly, with the smaller time step $\Delta t = 0.005$ s the coupled problem behaves similarly to the other tested meshes and time steps. The vertical displacement at the tip shows in this case an average frequency $\bar{f} = 3.05$ Hz and maximum displacements $d_{max} = 1.15$ cm. Again and the amplitude is modulated by a higher frequency

wave.

The solution of the *finest* discretization converges to the published results with the smallest time step considered; however, the dependency of the result in the time discretization for a given mesh in a way that two different stable solutions are reached deserves further assessment. We consider to be particularly relevant the fact that for every FFT plot of those shown in Fig. 16 there are two peaks, which correspond to the frequencies $f_1 \approx 3$ Hz and $f_2 \approx 6$ Hz. Even the coarsest test case shows some higher frequency effects during the transient period at the beginning of the simulation, which in that particular case are later damped out.

It is common when dealing with Vortex-Induced Vibrations (VIV) generated by bluff bodies to use the non-dimensional Strouhal number $St = fH/U$ to characterize the frequency of the response.[65–67] For this test case with $H = 1$ cm and $U = 51.3$ cm/s, the Strouhal numbers for the two frequencies f_1 and f_2 under consideration are $St_1 = 0.058$ and $St_2 = 0.117$.

Hübner *et al.*, in a paper published in 2004,[68] solve a problem with very similar settings to those presented in Fig. 14 and Table 1. Their test case differs from the one tackled here in the structural settings, but also in the inflow velocity used, which is set to be 31.5 cm/s. They solve a simulation with a rigid structure, i.e., with no structural deformation, and a refined $\Delta t = 0.001$ s. Interestingly, they report that for the rigid case the square cylinder sheds vortices that lead to a periodic behavior and a frequency $f = 3.7$ Hz. The authors explain that the vortices move over the cantilever and alternate in size. That would result on an alternate forcing acting over the structure at the frequency of the shedding. The Strouhal number of this case, with $H = 1$ cm, $U = 31.5$ cm/s, and $f = 3.7$ Hz, is $St = 0.117$. This value agrees with our computed value of St_2. Moreover, a Fourier analysis of the forces acting over the cantilever when this is held rigid for the three meshes presented in this work results in peaks ranging from 5.15 to 5.5 Hz and their harmonics, thus a value of St ranging from 0.100 to 0.107.

The results obtained in this section are summarized in Table 3. For all cases except for the finest mesh with the larger time step, the results agree very well the literature. This latter case converges to a Strouhal number similar to that presented by Hübner *et al.*[68] for a rigid cantilever.

Table 3. Summary of results and convergence study

	Average frequency (Hz)	Max tip displ. (cm)	High freq. effects	Strouhal number
Wall and Ramm[63]	3.08	1.31	Yes	0.06
Matthies and Steindorf[41]	2.99	1.34	No	0.058
Dettmer and Peric[14]	2.96 - 3.31	1.1 - 1.4	Yes	0.058 - 0.065
Wood *et al.*[23]	2.78 - 3.125	1.1 - 1.2	No	0.054 - 0.061
Kassiotis *et al.*[26]	3.17	1.0	No	0.062
Habchi *et al.*[39]	3.25	1.02	-	0.063
Froehle and Persson[18]	3.18	1.12	Yes	0.062
Hübner *et al.*[68] (rigid cantilever)				0.117
Coarse, $\Delta t = 0.0075$ s	3.15	1.15	No	0.061
Coarse, $\Delta t = 0.005$ s	3.15	1.15	No	0.061
Fine, $\Delta t = 0.0075$ s	3.10	1.25	Yes	0.060
Fine, $\Delta t = 0.005$ s	3.11	1.21	Yes	0.060
Finest, $\Delta t = 0.0075$ s	6.0	0.23	-	0.117
Finest, $\Delta t = 0.005$ s	3.05	1.15	Yes	0.059

Therefore, we conclude that the higher frequency effects reported in several papers and that result in a modulation of the response of the cantilever are due to the vortex shedding frequency of the square cylinder. In order to capture these vortex shedding effects, it is necessary to refine the fluid domain up to a level of discretization that prevents the vortical structures from damping out. In those cases, even a stable state of the coupled system may occur at that higher frequency, as shown in Fig 16, c).

It should be noted that the vortex shedding effects for the benchmark test case are not locked in with the response of the cantilever, due to a difference in frequencies of about 3 Hz. The frequency of vibration

that has been reported in the literature corresponds, mainly, to the vibration of the structure, which by being much heavier than the fluid dominates the coupled phenomenon. Once the fluid loads become non-symmetric, the structure starts its movement. The combination of a low elasticity modulus and a small inertia results in the resonance of the cantilever with a large amplitude. The effects of the vortex shedding, which is determined by the shape of the bluff body upstream, are then small compared to the amplitude of the structural vibration. These effects may even be neglected for coarse fluid discretizations, as they are damped out once a stationary state is reached.

IV.C. Analysis of the coupled dynamics

In order to further understand the problem, some relevant parameters on the dynamics of the coupled solution, such as structural inertia and stiffness, will be analyzed in this section. For simplicity and faster convergence, they have been run using the *coarse* mesh, which we have shown to be able to capture the first mode of the problem for the benchmark test case, even though it damps out the higher frequency effects for that particular case. Convergence, however, will be demonstrated for two tested cases in which the vortex shedding frequency is coupled with the dynamics of the coupled problem. This analysis is also intended to demonstrate the robustness of the presented implementation.

IV.C.1. Structural properties

We have explained in the previous section that the dynamics of the coupled problem are governed by the structural behavior. In order to confirm this statement, a simple test has been carried out, which consists in analyzing the effects of solving the problem with a linear, structural model. The linear model, given that the cantilever reaches vertical deflections over a 25% of its length, is expected to provide a source of error from the structural perspective (see Fig. 18). This behavior would be expected to modify the fluid flow, as the length of the appendix would increase under linear assumptions for large displacements.

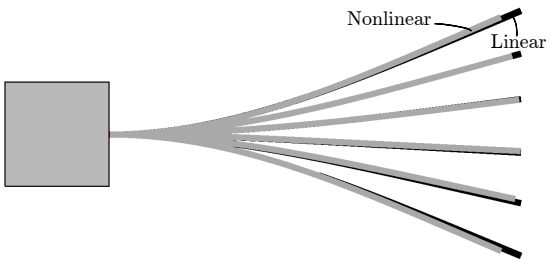

Figure 18. Differences in geometry of the cantilever beam when computed using a linear solver as opposed to a non-linear solver

However, a linear solver is still able to accurately compute the first bending mode of the structure and its frequency. In fact, the assumed natural frequency of 3.03 Hz for the cantilever corresponds to linear assumptions, while it is known that natural frequencies are slightly modified when accounting for geometrical non-linearities.[69]

The results obtained in section IV.B using a geometrically non-linear solver results will be compared with those obtained using a linear, structural solver, using the *coarse* configuration. We obtain the result shown in Fig. 19. It may be observed that the solution obtained using a linear solver is very close to the non-linear solution. The average frequency and the maximum tip displacement are respectively $\bar{f} = 3.13$ Hz and $d_{max} = 1.20$ cm, thus in line with the results in the open literature.

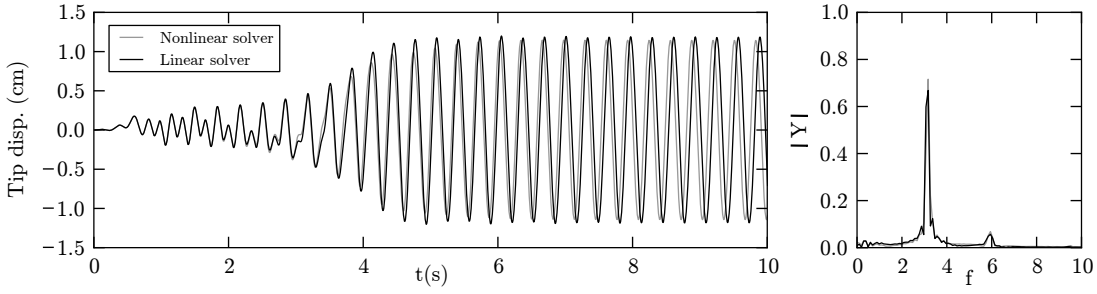

Figure 19. Time history and FFT plot for the linear structural model. Comparison with the non-linear model.

Another interesting consideration may be the study of the effects of the 2D formulation. It is well known

that there are two main approaches for bidimensional elasticity, namely, plane stress and plane strain. Assuming plane stress, the cantilever would be solved as if it were a thin plate with fluid loads only on its plane and unconstrained deformation in the third dimension. This has been the hypothesis adopted in this work, in order to compare with the results in literature. However, in order to use the problem as a benchmark for 3D cases applying symmetry boundary conditions, a plane strain case would be more appropriate. The behavior of the coupled problem is indeed affected by this assumption, as shown in Fig. 19. The average frequency measured using a plane strain assumption is $\bar{f} = 3.27$ Hz, while the maximum tip displacement is $d_{max} = 1.10$ cm.

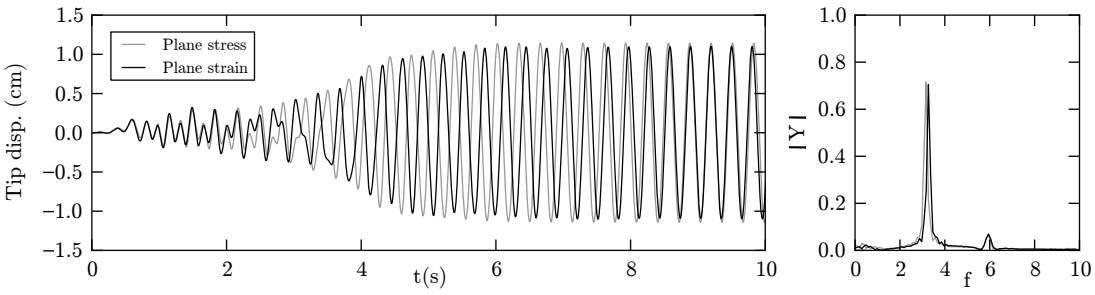

Figure 20. Time history and FFT plot for the 2D plane strain model. Comparison with the plane stress model.

IV.C.2. Structural density effects

The structural density has been modified in order to analyze the effects of the inertial effects of the structure. Four test cases have been run, using the *coarse* mesh. Assuming ρ_s=100 kg/m^3 as the reference structural density, the simulations have been run using $\frac{1}{2}\rho_s$, $\frac{3}{4}\rho_s$, $\frac{3}{2}\rho_s$, and $2\rho_s$. The Young's modulus E = 2.5 $\cdot 10^5$ Pa has also been scaled in the same proportion to maintain constant the first natural bending frequency.

The results are shown in Fig. 21. It may be observed that, as the structural density is increased, the transient time before the appendix reaches a stationary state on its first natural frequency is also increased. Lighter structures with smaller inertia, are induced to a resonant state by the the unsteady wake generated soon after the simulation is initialized. The structure vibrates mainly on its own first natural bending mode.

On the other hand, heavier structures take longer to reach this state. Their greater inertia makes it harder for the vibration state to develop. In particular, in the case of $2\rho_s$, this situation has not been reached in the 10 seconds of simulation. Interestingly, the appendix does vibrate with a much smaller amplitude of roughly 0.2 cm during this transient period. This phenomenon occurs at the vortex shedding frequency previously reported in section IV.B. The energy contained at this higher frequency of 6 Hz is for that case comparable with the contained at the natural frequency of 3 Hz. By the end of the simulation, however, it seems that the state of resonance is slowly developing.

IV.C.3. Frequency study

Finally, in a similar fashion as in the previous section, the influence of modifying the structural stiffness maintaining the structural density (thus, changing the bending frequency) has been further studied in this section. A range of linear frequencies from 2 to 10 Hz has been covered, and the results are shown in Fig. 22.

When the stiffness is reduced in order to match a natural bending frequency of 2 Hz, larger displacements and a smaller frequency are expected. This is shown in Fig. 22, a). The resonant state achieved is stationary, with no higher frequency effects: the structure is controlling the phenomenon and the vortex shedding frequency is damped out. However, by stiffening the structure over the limit of E = 2.5$\cdot 10^5$ Pa we obtain a coupled problem in which two frequencies are overlapping. The amplitude of the vibration is no longer stationary, and the frequency of the vortex shedding is no longer damped out even with the *coarse* spatial discretization. It is interesting to note that, as the structural properties are set to be more stiff, the frequency measured further differs from the linear estimation. This reflects the non-linearity of the coupled problem, including effects such as the added mass due to the density of the fluid. This is shown in Fig. 23.

This behavior reaches a limit for the test case f) in Fig. 22, which corresponds to a theoretical linear frequency of 7 Hz, thus a Young's modulus E = 1.34 $\cdot 10^6$ Pa. This is also shown in Fig. 23. The solution

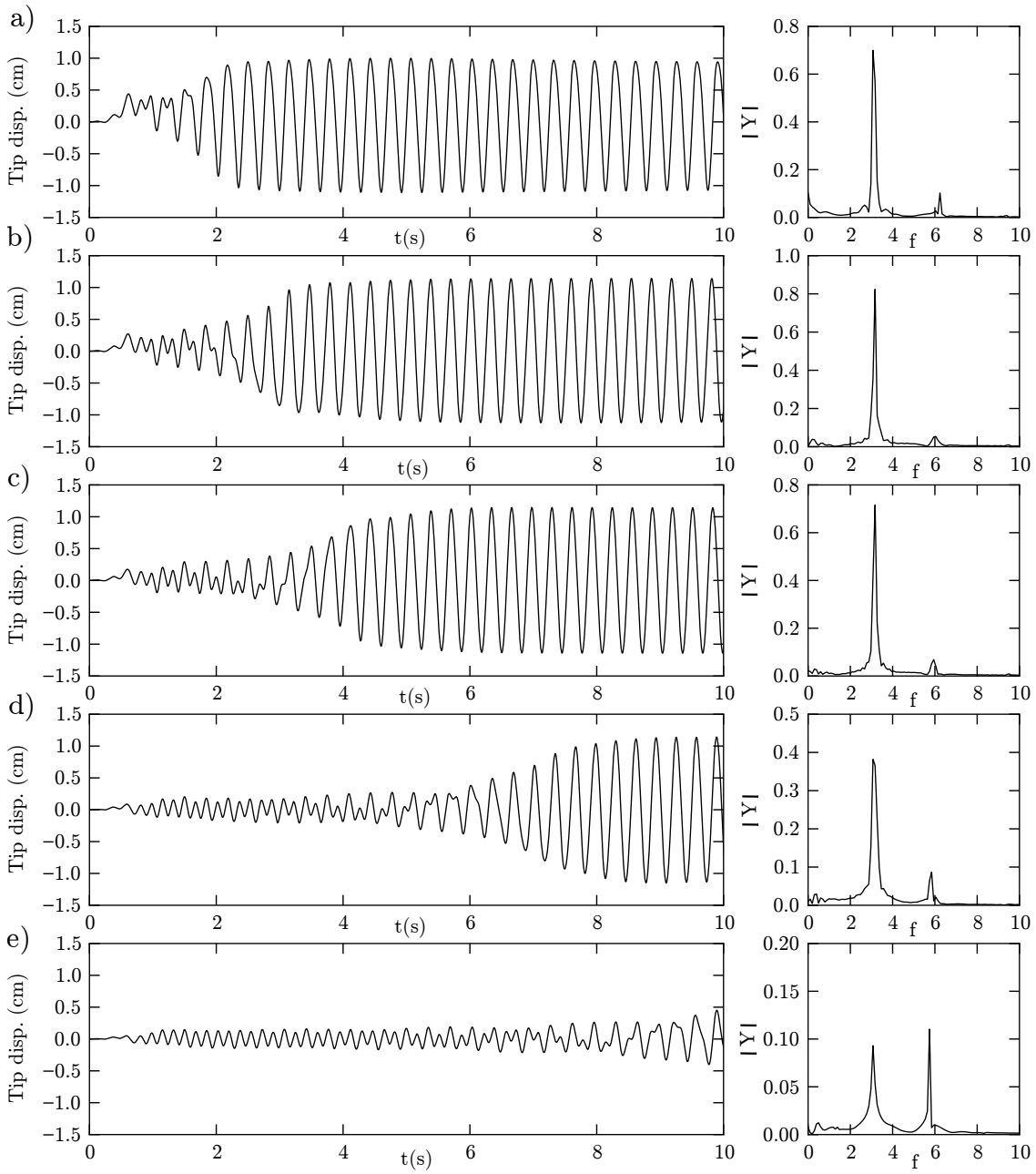

Figure 21. Study of the effects of varying the mass ratio. Time histories and FFT plots for the following structural densities (stiffness scaled in the same proportion to maintain the first bending frequency): a) ρ_s = 50 kg/m^3 b) ρ_s = 75 kg/m^3 c) Reference, ρ_s = 100 kg/m^3 d) ρ_s = 150 kg/m^3 e) ρ_s = 200 kg/m^3.

obtained is apparently locked in, with vibrations occurring at a frequency of 5.04 Hz. The frequency of the coupled problem shows now a strong influence from the fluid behavior, as opposed to the test case presented in section IV.B. This stable coupled behavior is also obtained when a test case with a Young's modulus E = $2.75 \cdot 10^6$ Pa, and therefore a theoretical linear frequency of 10 Hz, is run. We then obtain a coupled state with a mean frequency of 5.31 Hz. Given that both of these test cases were run using the *coarse* discretization, a convergence analysis was run for each test case to ensure that the solution obtained was converged. This is shown in Fig. 24 and Fig. 25, where convergence is demonstrated. The relevant magnitudes obtained for both test cases are reported in table 4.

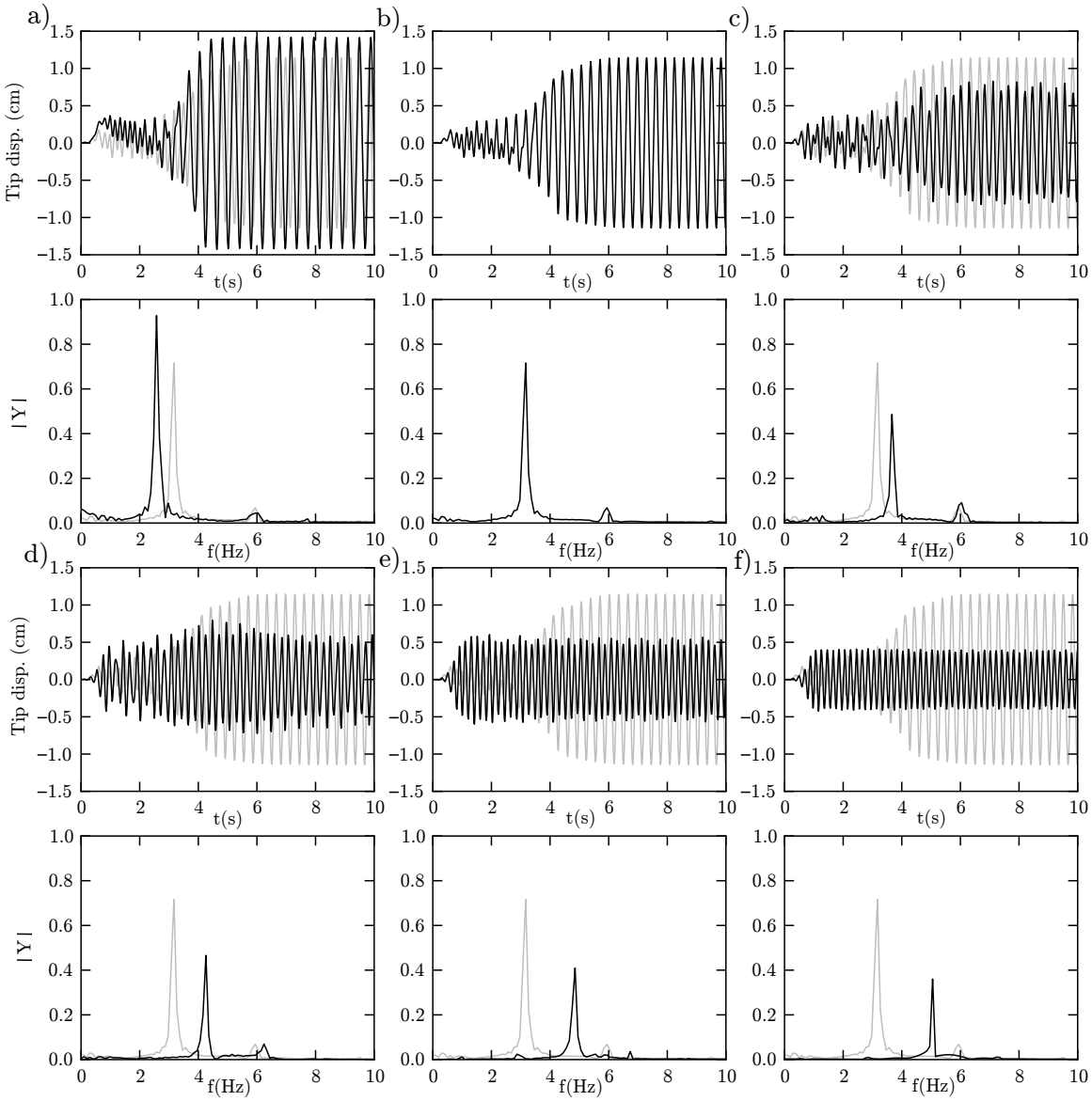

Figure 22. Frequency study. Time histories and FFT plots for the following Young's modulus, which correspond to theoretical first bending frequencies of 2, 3, 4, 5, 6 and 7 Hz respectively: a) E = 1.1 $\cdot 10^5$ Pa. b) Reference, E = 2.5 $\cdot 10^5$ Pa. c) E = 4.4 $\cdot 10^5$ Pa. d) E = 6.8 $\cdot 10^5$ Pa. e) E = 1 $\cdot 10^6$ Pa. f) E = 1.34 $\cdot 10^6$ Pa. The reference case is plotted in the background of the remaining plots for comparison purposes.

Table 4. Convergence study for two test cases with theoretical frequencies of 7 and 10 Hz.

		Average frequency (Hz)	Max tip displ. (cm)	Strouhal number
	Coarse	5.04 - 5.07	0.40	0.098 - 0.099
E = 1.34 $\cdot 10^6$ Pa	Fine	5.00 - 5.05	0.40 - 0.41	0.097 - 0.098
	Finest	5.02 - 5.05	0.39	0.098
	Coarse	5.31 - 5.37	0.12	0.104 - 0.105
E = 2.75 $\cdot 10^6$ Pa	Fine	5.31 - 5.36	0.13	0.104
	Finest	5.32 - 5.38	0.13	0.104 - 0.105

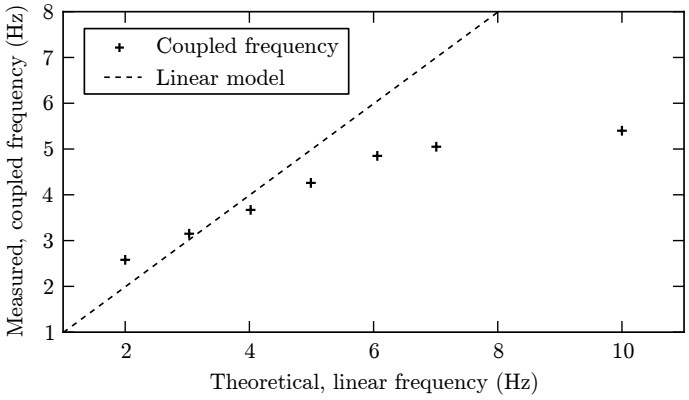

Figure 23. Frequency study. Theoretical frequency from a linear structural analysis compared with the measured frequency of the coupled system.

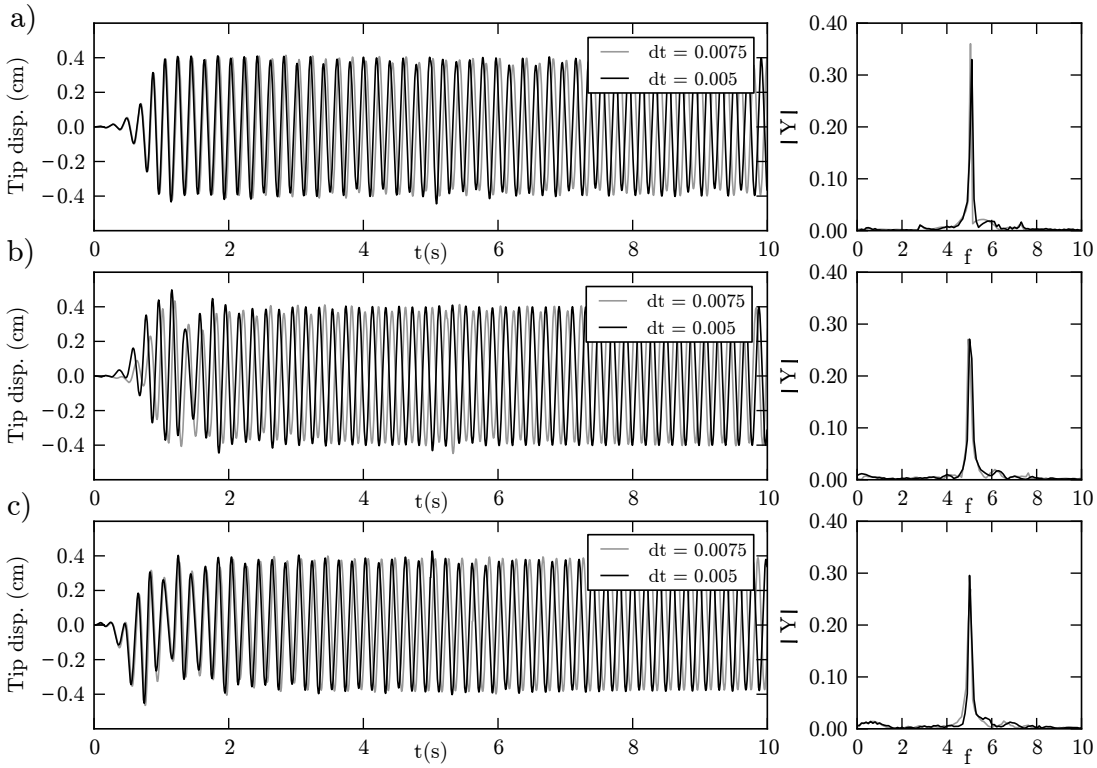

Figure 24. Test case with E = 1.34 $\cdot 10^6$ Pa. Time histories of the vertical displacements at the tip of the cantilever and FFT plots, for the a) *coarse*, b) *fine* and c) *finest* fluid discretizations, and the two time steps considered, Δt = 0.0075 s and Δt = 0.005 s

V. Conclusions

Structural dynamics and Fluid-Structure Interaction capabilities have been implemented into the open-source SU2 suite. A Finite Element structural solver, able to deal with both geometrical and material non-linearities, has been natively embedded into the core of SU2. The original philosophy of modularity of the code has been maintained, by employing and expanding the object-oriented architecture of the main solver. In particular, a new set of classes were designed and implemented, in order to serve as the basis for further FE-based applications. High levels of abstraction have been used in the design of the structural solver to ease future developments.

The same idea has been maintained in the development of new structures able handle the different

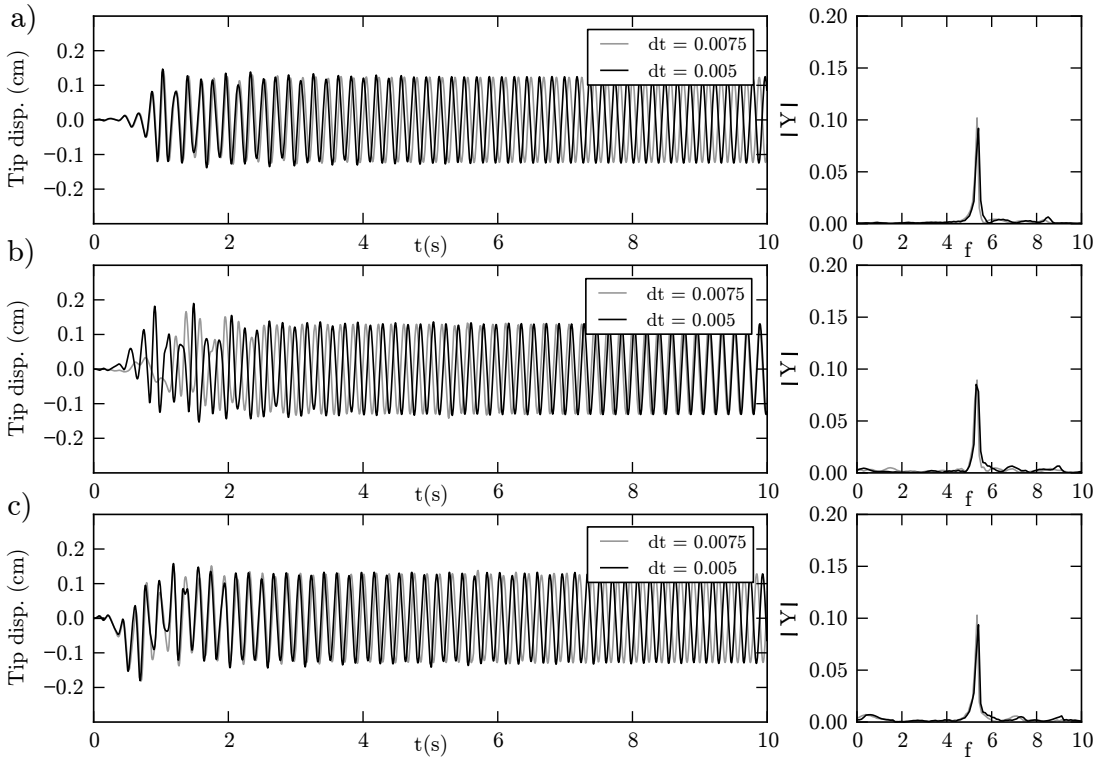

Figure 25. Test case with E = 2.75 $\cdot 10^6$ Pa. Time histories of the vertical displacements at the tip of the cantilever and FFT plots, for the a) *coarse*, b) *fine* and c) *finest* fluid discretizations, and the two time steps considered, $\Delta t = 0.0075$ s and $\Delta t = 0.005$ s

solvers in the code within a single instance of SU2. In particular, new classes have been built for driving the simulation, transferring the information and interpolating the information between different spatial discretizations. For the particular problem of Fluid-Structure Interaction, a Block-Gauss-Seidel approach with dynamic relaxation parameters has been implemented, thus solving the problem in strongly-coupled, partitioned way.

The Fluid-Structure Interaction capabilities developed in this work have been tested by solving a Vortex-Induced Vibration problem that has been widely used throughout the literature as a benchmark for FSI solvers. The results obtained in this work are in very good agreement with the relevant literature. Moreover, we provide a clear and concise review of the state of the art for the relevant phenomena and dynamics of the problem.

Acknowledgements

Ruben Sanchez and Rafael Palacios gratefully acknowledge the financial support of the European Office of Aerospace Research & Development of the US Air Force Office of Scientific Research, and the UK Engineering and Physical Sciences Research Council Grant EP/J002070/1, "Towards Biologically-Inspired Active-Compliant-Wing Micro-Air-Vehicles".

The commitment of the SU2 development team at the Aerospace Design Laboratory at Stanford University to maintain the open-source nature of the software encourages the community to engage in the improvement, validation and further development of the code.

References

[1]Farhat, C., Lesoinne, M., and LeTallec, P., "Load and motion transfer algorithms for fluid/structure interaction problems with non-matching discrete interfaces: Momentum and energy conservation, optimal discretization and application to aeroelasticity," *Computer Methods in Applied Mechanics and Engineering*, Vol. 157, No. 1-2, 1998, pp. 95–114.

[2]Beckert, A., "Coupling fluid (CFD) and structural (FE) models using finite interpolation elements," *Aerospace Science*

and Technology, Vol. 4, No. 1, 2000, pp. 13–22.

[3]Farhat, C., van der Zee, K., and Geuzaine, P., "Provably second-order time-accurate loosely-coupled solution algorithms for transient nonlinear computational aeroelasticity," *Computer Methods in Applied Mechanics and Engineering*, Vol. 195, No. 17-18, 2006, pp. 1973–2001.

[4]Palacios, R., Murua, J., and Cook, R., "Structural and aerodynamic models in nonlinear flight dynamics of very flexible aircraft," *AIAA Journal*, Vol. 48, No. 11, 2010, pp. 2648–2659.

[5]Murua, J., Palacios, R., and Graham, J., "Assessment of wake-tail interference effects on the dynamics of flexible aircraft," *AIAA Journal*, Vol. 50, No. 7, 2012, pp. 1575–1585.

[6]Deparis, S., Discacciati, M., Fourestey, G., and Quarteroni, A., "Fluid-structure algorithms based on Steklov-Poincaré operators," *Computer Methods in Applied Mechanics and Engineering*, Vol. 195, No. 41-43, 2006, pp. 5797–5812.

[7]Fernández, M., Gerbeau, J.-F., and Grandmont, C., "A projection semi-implicit scheme for the coupling of an elastic structure with an incompressible fluid," *International Journal for Numerical Methods in Engineering*, Vol. 69, No. 4, 2007, pp. 794–821.

[8]Carstens, V., Kemme, R., and Schmitt, S., "Coupled simulation of flow-structure interaction in turbomachinery," *Aerospace Science and Technology*, Vol. 7, No. 4, 2003, pp. 298–306.

[9]Campbell, R. and Paterson, E., "Fluid-structure interaction analysis of flexible turbomachinery," *Journal of Fluids and Structures*, Vol. 27, No. 8, 2011, pp. 1376–1391.

[10]Belytschko, T., "Fluid-structure interaction," *Computers & Structures*, Vol. 12, No. 4, 1980, pp. 459 – 469.

[11]Farhat, C. and Lesoinne, M., "Two efficient staggered algorithms for the serial and parallel solution of three-dimensional nonlinear transient aeroelastic problems," *Computer Methods in Applied Mechanics and Engineering*, Vol. 182, No. 34, 2000, pp. 499–515.

[12]Le Tallec, P. and Mouro, J., "Fluid structure interaction with large structural displacements," *Computer Methods in Applied Mechanics and Engineering*, Vol. 190, No. 24-25, 2001, pp. 3039–3067.

[13]Guruswamy, G., "A review of numerical fluids/structures interface methods for computations using high-fidelity equations," *Computers and Structures*, Vol. 80, No. 1, 2002, pp. 31–41.

[14]Dettmer, W. and Perić, D., "A computational framework for fluid-structure interaction: Finite element formulation and applications," *Computer Methods in Applied Mechanics and Engineering*, Vol. 195, No. 41-43, 2006, pp. 5754–5779.

[15]Küttler, U., Gee, M., Förster, C., Comerford, A., and Wall, W., "Coupling strategies for biomedical fluid-structure interaction problems," *International Journal for Numerical Methods in Biomedical Engineering*, Vol. 26, No. 3-4, 2010, pp. 305–321.

[16]Bazilevs, Y., Takizawa, K., and Tezduyar, T., *Computational Fluid-Structure Interaction: Methods and Applications*, John Wiley & Sons, Ltd, The Atrium, Southern Gate, Chichester, West Sussex, PO10 8SQ, UK, 2013.

[17]Bazilevs, Y., Hsu, M.-C., and Scott, M., "Isogeometric fluidstructure interaction analysis with emphasis on non-matching discretizations, and with application to wind turbines," *Computer Methods in Applied Mechanics and Engineering*, Vol. 249252, No. 0, 2012, pp. 28 – 41.

[18]Froehle, B. and Persson, P.-O., "A high-order discontinuous Galerkin method for fluid-structure interaction with efficient implicit-explicit time stepping," *Journal of Computational Physics*, Vol. 272, 2014, pp. 97–104.

[19]Casquero, H., Bona-Casas, C., and Gomez, H., "A NURBS-based immersed methodology for fluid-structure interaction," *Computer Methods in Applied Mechanics and Engineering*, Vol. 284, 2015, pp. 943–970.

[20]Palacios, F., Colonno, M., Aranake, A., Campos, A., Copeland, S., Economon, T., Lonkar, A., Lukaczyk, T., Taylor, T., and Alonso, J., "Stanford University Unstructured (SU2): An open-source integrated computational environment for multi-physics simulation and design," *AIAA 51st Aerospace Sciences Meeting, 7-10 January*, Grapevine, TX, 2013.

[21]Palacios, F., Economon, T., Aranake, A., Copeland, S., Lonkar, A., Lukaczyk, T., Manosalvas, D., Naik, K., Santiago Padrón, A., Tracey, B., Variyar, A., and Alonso, J., "Stanford university unstructured (SU2): Open-source analysis and design technology for turbulent flows," *AIAA 52nd Aerospace Sciences Meeting, SciTech, 13-17 January*, National Harbor, MD, 2014.

[22]Economon, T., Palacios, F., Alonso, J., Bansal, G., Mudigere, D., Deshpande, A., Heinecke, A., and Smelyanskiy, A., "Towards High-Performance Optimizations of the Unstructured Open-Source SU2 Suite," *AIAA 53rd Aerospace Sciences Meeting, Scitech, 5-9 January*, Kissimmee , FL, 2015.

[23]Wood, C., Gil, A., Hassan, O., and Bonet, J., "A partitioned coupling approach for dynamic fluid-structure interaction with applications to biological membranes," *International Journal for Numerical Methods in Fluids*, Vol. 57, No. 5, 2008, pp. 555–581.

[24]Heil, M., Hazel, A., and Boyle, J., "Solvers for large-displacement fluid-structure interaction problems: Segregated versus monolithic approaches," *Computational Mechanics*, Vol. 43, No. 1, 2008, pp. 91–101.

[25]Piperno, S. and Farhat, C., "Partitioned procedures for the transient solution of coupled aeroelastic problems Part II: energy transfer analysis and three-dimensional applications," *Computer Methods in Applied Mechanics and Engineering*, Vol. 190, No. 2425, 2001, pp. 3147–3170.

[26]Kassiotis, C., Ibrahimbegovic, A., Niekamp, R., and Matthies, H., "Nonlinear fluid-structure interaction problem. Part I: Implicit partitioned algorithm, nonlinear stability proof and validation examples," *Computational Mechanics*, Vol. 47, No. 3, 2011, pp. 305–323.

[27]Donea, J., Giuliani, S., and Halleux, J., "An arbitrary lagrangian-eulerian finite element method for transient dynamic fluid-structure interactions," *Computer Methods in Applied Mechanics and Engineering*, Vol. 33, No. 1-3, 1982, pp. 689–723.

[28]Donea, J., Huerta, A., Ponthot, J.-P., and Rodríguez-Ferran, A., *Encyclopedia of Computational Mechanics*, chap. Arbitrary Lagrangian-Eulerian Methods, John Wiley & Sons, Ltd, 2004.

[29]Hojjat, M., Stavropoulou, E., Gallinger, T., Israel, U., Wüchner, R., and K.-U., B., *Fluid Structure Interaction II*, Vol. 73, chap. Fluid-Structure Interaction in the Context of Shape Optimization and Computational Wind Engineering, Springer Berlin Heidelberg, 2010, pp. 351–381.

[30]Hughes, T. J. R., *The Finite Element Method: Linear Static and Dynamic Finite Element Analysis*, Englewood Cliffs, N.J. Prentice-Hall International, 1987.

[31]Farhat, C., Lesoinne, M., Stern, P., and Lantéri, S., "High performance solution of three-dimensional nonlinear aeroelastic problems via parallel partitioned algorithms: Methodology and preliminary results," *Advances in Engineering Software*, Vol. 28, No. 1, 1997, pp. 43–61.

[32]Jaiman, R., Geubelle, P., Loth, E., and Jiao, X., "Combined interface boundary condition method for unsteady fluid-structure interaction," *Computer Methods in Applied Mechanics and Engineering*, Vol. 200, No. 1-4, 2011, pp. 27–39.

[33]Dettmer, W. and Perić, D., "A new staggered scheme for fluid-structure interaction," *International Journal for Numerical Methods in Engineering*, Vol. 93, No. 1, 2013, pp. 1–22.

[34]Von Scheven, M. and Ramm, E., "Strong coupling schemes for interaction of thin-walled structures and incompressible flows," *International Journal for Numerical Methods in Engineering*, Vol. 87, No. 1-5, 2011, pp. 214–231.

[35]Causin, P., Gerbeau, J., and Nobile, F., "Added-mass effect in the design of partitioned algorithms for fluid-structure problems," *Computer Methods in Applied Mechanics and Engineering*, Vol. 194, No. 42-44, 2005, pp. 4506–4527.

[36]Matthies, H. G. and Steindorf, J., "Partitioned but strongly coupled iteration schemes for nonlinear fluidstructure interaction," *Computers & Structures*, Vol. 80, No. 2730, 2002, pp. 199–1999.

[37]Küttler, U. and Wall, W., "Fixed-point fluid-structure interaction solvers with dynamic relaxation," *Computational Mechanics*, Vol. 43, No. 1, 2008, pp. 61–72.

[38]Degroote, J., Bathe, K.-J., and Vierendeels, J., "Performance of a new partitioned procedure versus a monolithic procedure in fluid-structure interaction," *Computers and Structures*, Vol. 87, No. 11-12, 2009, pp. 793–801.

[39]Habchi, C., Russeil, S., Bougeard, D., Harion, J.-L., Lemenand, T., Ghanem, A., Valle, D., and Peerhossaini, H., "Partitioned solver for strongly coupled fluid-structure interaction," *Computers and Fluids*, Vol. 71, 2013, pp. 306–319.

[40]Irons, B. M. and Tuck, R. C., "A version of the Aitken accelerator for computer iteration," *International Journal for Numerical Methods in Engineering*, Vol. 1, 1969, pp. 275–277.

[41]Matthies, H. G. and Steindorf, J., "Partitioned strong coupling algorithms for fluidstructure interaction," *Computers & Structures*, Vol. 81, No. 811, 2003, pp. 805–812.

[42]Vierendeels, J., Lanoye, L., Degroote, J., and Verdonck, P., "Implicit coupling of partitioned fluid-structure interaction problems with reduced order models," *Computers and Structures*, Vol. 85, No. 11-14, 2007, pp. 970–976.

[43]Cebral, J. and Löhner, R., "Conservative load projection and tracking for fluid-structure problems," *AIAA Journal*, Vol. 35, No. 4, 1997, pp. 687–692.

[44]Smith, M., Hodges, D., and Cesnik, C., "Evaluation of computational algorithms suitable for fluid-structure interactions," *Journal of Aircraft*, Vol. 37, No. 2, 2000, pp. 282–294.

[45]de Boer, A., van Zuijlen, A., and Bijl, H., "Review of coupling methods for non-matching meshes," *Computer Methods in Applied Mechanics and Engineering*, Vol. 196, No. 8, 2007, pp. 1515–1525.

[46]Jiao, X. and Heath, M., "Overlaying surface meshes, part I: Algorithms," *International Journal of Computational Geometry and Applications*, Vol. 14, No. 6, 2004, pp. 379–402.

[47]Jaiman, R., Jiao, X., Geubelle, P., and Loth, E., "Assessment of conservative load transfer for fluid-solid interface with non-matching meshes," *International Journal for Numerical Methods in Engineering*, Vol. 64, No. 15, 2005, pp. 2014–2038.

[48]Beckert, A. and Wendland, H., "Multivariate interpolation for fluid-structure-interaction problems using radial basis functions," *Aerospace Science and Technology*, Vol. 5, No. 2, 2001, pp. 125–134.

[49]Brown, S., "Displacement extrapolations for CFD+CSM aeroelastic analysis," Vol. 1, AIAA, New York, NY, United States, Kissimmee, FL, USA, 1997, pp. 291–300.

[50]Breuer, M., De Nayer, G., Münsch, M., Gallinger, T., and Wüchner, R., "Fluid-structure interaction using a partitioned semi-implicit predictor-corrector coupling scheme for the application of large-eddy simulation," *Journal of Fluids and Structures*, Vol. 29, 2012, pp. 107–130.

[51]Jiao, X. and Heath, M., "Common-refinement-based data transfer between non-matching meshes in multiphysics simulations," *International Journal for Numerical Methods in Engineering*, Vol. 61, No. 14, 2004, pp. 2402–2427.

[52]Jaiman, R., Jiao, X., Geubelle, P., and Loth, E., "Conservative load transfer along curved fluid-solid interface with non-matching meshes," *Journal of Computational Physics*, Vol. 218, No. 1, 2006, pp. 372–397.

[53]Jaiman, R., Geubelle, P., Loth, E., and Jiao, X., "Transient fluid-structure interaction with non-matching spatial and temporal discretizations," *Computers and Fluids*, Vol. 50, No. 1, 2011, pp. 120–135.

[54]Farrell, P. and Maddison, J., "Conservative interpolation between volume meshes by local Galerkin projection," *Computer Methods in Applied Mechanics and Engineering*, Vol. 200, No. 1-4, 2011, pp. 89–100.

[55]Wendland, H., "Piecewise polynomial, positive definite and compactly supported radial functions of minimal degree," *Advances in Computational Mathematics*, Vol. 4, No. 1, 1995, pp. 389–396.

[56]Jameson, A., "Time dependent calculations using multigrid, with applications to unsteady flows past airfoils and wings," *AIAA 10th Computational Fluid Dynamics Conference, June 24-26*, Honolulu, HI, 1991.

[57]Bathe, K.-J., *Finite Element Procedures in Engineering Analysis*, Civil engineering and engineering mechanics series, Prentice-Hall, 1982.

[58]Bonet, J. and Wood, R. D., *Nonlinear Continuum Mechanics for Finite Element Analysis*, Cambridge University Press, 1997.

[59]Newmark, N. M., "A Method of Computation for Structural Dynamics," *Journal of the Engineering Mechanics Division*, Vol. 85, No. 3, 1959, pp. 67–94.

[60]Chung, J. and Hulbert, G., "Time integration algorithm for structural dynamics with improved numerical dissipation: the generalized-α method," *Journal of Applied Mechanics, Transactions ASME*, Vol. 60, No. 2, 1993, pp. 371–375.

[61]Kline, H., Palacios, F., and Alonso, J., "Sensitivity of the Performance of a 3-Dimensional Hypersonic Inlet to Shape Deformations," *AIAA 19th International Space Planes and Hypersonic Systems and Technologies Conference, 16-20 June*, Atlanta, GA, 2014.

[62]Dwight, R., "Robust mesh deformation using the linear elasticity equations," Springer Berlin, Ghent, 2009, pp. 401–406.

[63]Wall, W. and Ramm, E., "Fluid-Structure interaction based upon a stabilized (ALE) finite element method." *Computational Mechanics. New Trends and Applications*, edited by E. O. n. S.R. Idelsohn and E. D. (Eds.), CIMNE, Barcelona, Spain, 1998.

[64]Geuzaine, C. and Remacle, J.-F., "Gmsh: A 3-D finite element mesh generator with built-in pre- and post-processing facilities," *International Journal for Numerical Methods in Engineering*, Vol. 79, No. 11, 2009, pp. 1309–1331.

[65]Simiu, E. and Scanlan, R. H., *Wind effects on Structures: Fundamentals and Applications to Design*, John Wiley &Sons, 3rd ed., 1996.

[66]Jurado, J., Sanchez, R., and Hernández, S., "Wind tunnel sectional tests for the identification of flutter derivatives and vortex shedding in long span bridges," Vol. 129, Gran Canaria, 2013, pp. 51–59.

[67]Sanchez, R., Nieto, F., Kwok, K., and Hernández, S., "CFD Analysis of the aerodynamic response of a twin-box deck considering different gap widths," *Congresso de Métodos Numéricos em Engenharía 2015*, edited by Apmtac, Lisbon, Portugal, June-July 2015.

[68]Hübner, B., Walhorn, E., and Dinkler, D., "A monolithic approach to fluid-structure interaction using space-time finite elements," *Computer Methods in Applied Mechanics and Engineering*, Vol. 193, No. 23-26, 2004, pp. 2087–2104.

[69]Palacios, R., "Nonlinear normal modes in an intrinsic theory of anisotropic beams," *Journal of Sound and Vibration*, Vol. 330, No. 8, 2011, pp. 1772–1792.